Desalination processes of thin sea ice during freezing and melting

Luise Marie Zeigermann

December 18, 2018

Master's thesis Physical Oceanography
University Hamburg

1. Supervisor: Dr. Dirk Notz
2. Supervisor: Prof. Dr. Johanna Baehr

Desalination processes during melting and freezing

Abstract

Sea ice is an inhomogeneous continuum of solid ice crystals, liquid highly saline brine and gas bubbles. The solid fraction and bulk salinity of sea ice determine its dynamical and dielectric properties which are influencing large-scale measurements of sea-ice properties by satellites. The salt drains out of the ice due to desalination processes, gravity drainage during freezing and flushing during melting. The physics of desalination are poorly understood so far due to sparse continuous measurements and only a few sea-ice model implementations. This thesis presents and discusses several laboratory experiments of freezing and melting artificial sea ice in a cooling chamber. The temporal evolution of solid fraction, ice temperature and bulk salinity in growing sea ice, up to 16 cm, was observed continuously in a 2 cm vertical resolution by a so-called wireharp. The experiments were simulated with a 1-D sea-ice model, called SAMSIM, to investigate the agreement of the implemented physical description of desalination in a model with the measurements. During freezing, the bulk salinity decreases and the a vertical profile evolves which show a low salinity of about 5-7 g/kg in the interior of the ice and an increase towards the ice bottom. SAMSIM is able to simulate the measured shapes of the temporally evolving profiles of bulk salinity and solid fraction but its slightly underestimates the solid fraction and overestimates bulk salinity by about 2-5 g/kg. Experiments with several wireharps show that the bulk salinity and solid fraction evolve spatially inhomogeneous caused by non-uniform ice temperatures across the artificial sea ice. SAMSIM was not able to simulate the differences in solid fraction and bulk salinity due to the temperature difference. The melting experiments provide the first continuous measurements of solid fraction and bulk salinity during melting. It was observed that the ice temperature becomes homogeneous and that the bulk salinity decreases slightly in upper layers what goes along with a slight increase in solid fraction. For sea ice, thinner than 12 cm, the solid fraction decreases almost in all ice depths simultaneously and the bulk salinity in the interior increases, very likely due to a replacement of melt water by salty water form below the ice. SAMSIM is not able to simulate the measured profiles because its flushing parameterization is based on assumptions which could not be found in the measurements. These melting experiments could be used to adapt SAMSIM's flushing parameterization for thin sea ice and in a further context could reduce the uncertainty of satellite measurements in summer.

Contents

1 Introduction

Sea ice is frozen sea water but it is less saline. During freezing, salt cannot be incorporated into the solid ice-crystal structure. The salt remains as highly saline brine in the interstices between the freshwater ice crystals. The concentration of brine depends on the ice temperature because the freezing temperature depends on the salinity of seawater (Assur, 1958). Over time, the brine drains out due to the potential-energy difference between brine and saltwater (so-called gravity drainage) and freshwater flushing in summer (Notz and Worster, 2009).

When brine is rejected into the underlying ocean, the density of seawater and the vertical stratification of the ocean is influenced. The exchange of salt between sea ice and seawater therefore contributes to water mass formation and influences ocean circulations across hundreds of kilometers, specially in the Arctic, where changes in salinity affect ocean's density more than changes in temperature (Aargaard and Carmack, 1989).

Salt in sea ice is also important on very small scales. Sea ice is not a lifeless medium rather it is colonized by sympagic bacteria, algae and photo-and metazoans (Horner, 1985 and 1990). The life in sea ice concentrates in the brine-channel system as its walls constitute large surface areas that are used as attachment, locomotion and grazing for living organism. Since the geometry of brine channels occur in dependence to physical changes in liquid fraction, the space which can be colonized and biogeochemical processes are directly linked to changes in temperature and salinity of sea ice (Krembs et al., 1999).

The most used technique to observe sea-ice salinity is by direct measurements of ice cores. After taking an ice core, it is divided into sections which are melted afterwards. Hence, it is possible to measure the bulk salinity respective to the ice depth. The drawbacks of this method are brine drainage while removing the core out of its hydrostatic equilibrium, short continuous time series and it is not possible to observe temporally varying salinity profiles in situ (Notz et al., 2005).

Ice-core measurements show different salinity profiles for sea ice during freezing and melting because sea ice is continuous in salinity and solid fraction. The salinity profile of Arctic first-year ice was found to be C-shaped, what means, a higher salinity at the ice surface than in the interior and an increase in salinity towards the ice bottom (e.g Nakawo and Sinha, 1981). In absolute values, it could be mea-

sured that the salinity is decreasing from 20 ‰ and 10 ‰ when sea-ice thickness has reached about 30 cm (Kovacs, 1996). Information about the salinity of melting first-year Arctic sea ice are rare. From ice-core measurements in the Fram strait region, Tucker et al. (1987) found that a strong desalination occurs at the ice surface during melting from about June to July.

As an first approach for in situ measurements, Cox and Weeks (1975) grew ice from a radioactive sodium-chloride solution and determined the evolution of salinity distribution in 1 cm spatial resolution over a 16 hours. This method is just possible as an laboratory experiment and not suitable for field observations. Another used technique is time-domain spectroscopy and capacitance measurements which allow determining the liquid fraction in an amount of partially frozen systems, by measuring absorption of electromagnetic waves through a sample of sea ice and determining the liquid fraction. By measuring the vertical temperature profile it is possible to define the the existing salinity with cm resolution (e.g. Campbell, 1990).

Notz et al. (2005) introduced a measurement device, hereafter referred as wireharp which can be used for continuous in situ measurements of solid fraction and temperature in sea ice. It is based on the assumption, that pure is ice is a very good electrical insulator and that the electrical resistance of sea ice increases proportional to its solid fraction. The instrument has a spatial resolution of 2 cm and and is suitable for measurements in thin sea ice. Due to its high temporal resolution, continuous recording and simple implementation, the wireharp is an appropriate measuring device for field campaigns and laboratory experiments.

As continuous measurements of salinity in growing sea ice are sparse, I let artificial sea ice grow and melt in a glass tank to study desalination. I used a wireharp to determine the temporal evolution of solid fraction and salinity profiles in thin sea ice. These kind of laboratory experiments are unique as they provide continuous in-situ measurements of solid fraction and salinity with a high temporal resolution of artificial sea ice which grew and melt under relatively near-natural conditions: free-floating ice, a free air/ice interface and a well mixed salty water column. The proceeded experiments show how suitable and reliable the measurements of the wireharp are to understand desalination during freezing and melting.

Sea ice can have a high horizontal heterogeneity in salinity (below about 10 cm) caused by the location and morphology of brine channels (Cottier et al., 1999).

Variability that occurs at 2-20 m scale is controlled by variability in brine drainage (Eicken et al. 1991). Due to this heterogeneity, ice-core measurements has to be regarded with a certain uncertainty if they are treated as representative for a larger region from where they were taken. To study the heterogeneity of sea ice I performed experiments whereby I measured the solid fraction and ice temperature at 3 different locations (about 0.3 m distance) in sea ice in one single tank. From these measurements I can estimate reasons for similarities and differences in the temperature, salinity and solid fraction profiles across the artificial sea ice.

Measurement campaigns in the Arctic and Antarctic as well as lab measurements are sparse because they are expensive and time-consuming. It is therefore indispensable to perform model studies as it is much easier to create a diversity of boundary conditions and long terms. Currently, desalination is not implemented in the sea-ice component of global earth system models (GESMs). For example, the MPI-ESM (Max-Planck-Institute Earth System Model) includes sea-ice thermodynamics, snow accumulation along with snow-ice transformation but the salinity is assumed as constantly 5 g/kg for freezing and melting (Jungclaus et al, 2013). Sea-ice is a continuum of salty brine and fresh ice. The assumption of a constant salinity will inevitably lead to a loss of information about the thermodynamical properties. On the other hand it is still unclear how much sophisticated a salinity parameterization should become to not exceed computational cost and code complexity in contrast to a few improvements (Griewank and Notz, 2015). It is therefore convenient to invent and improve sea-ice models with simple parameterizations to test the suspected physical processes which are causing desalination during freezing and melting.

I simulated the proceeded freezing experiments with a 1-D sea-ice model, called SAMSIM (Griewank, 2013). It includes a thermodynamic core, gas phase and a parameterization for gravity drainage. The model was forced with the experimental ice-surface temperature and a heat flux from the water. The included sea-ice thermodynamics were very likely able to reproduce the measured ice temperature. A comparison between modeled and measured salinity and solid-fraction profiles could therefore be used to investigate how far the implemented gravity-drainage parameterization is able to reproduce the evolution of solid fraction and salinity during freezing.

The lab measurements only cover very thin sea ice. But thin sea ice could become more frequent as satellites observed that the arctic sea ice becomes thinner

and the extent in winter and summer has shrunk significantly over the last few decades (NSIDC, 2018a). This decrease in sea ice is related to climate change and is supposed to continue in future. For the coming decades, the arctic sea ice is expected to become younger and thinner and the seasonal variety of sea ice could increase (Vaughan et al., 2013). Thin first-year ice could therefore become more and more present in the central Arctic and freezing and melting could become more frequently.

Satellite measurements are the measuring instruments which collect highly-resolved data of thickness, extent and other parameters of sea ice in Arctic and Antarctic. The measurements are based on the understanding of the thermodynamic and dielectric properties of sea ice which are determined by solid fraction and salinity amongst other things. For example, the short wave radiation is scattered in the ice and is therefore affected by the size and the shape of the brine-channel system (Perovich, 1998). The relatively small-scale lab measurements and model studies, I performed, could therefore also contribute to an improvement of large-scale measurements.

There do not exist continuous measurements of salinity and solid fraction in melting sea ice. The physical processes at the surface and in the interior of the ice are poorly understood so far as there is only a sparse amount of ice-core measurements from the melting season (e.g. Eicken, 2002). Satellite measurements have therefore a higher uncertainty in summer than in winter (Yang et al. 2016). The melting experiments, I performed under near-natural conditions, provide the first continuous measurements of salinity and solid fraction during melting. From these experiments, I can identify physical processes occurring at the ice surface and the ice bottom during melting.

Griewank and Notz (2015) introduced a flushing parameterization for SAMSIM. This parameterization was found to be able to simulate the salinity profile of sea-ice cores which were taken during the melting season at Point Barrow, Alaska (Eicken et al., 2002). My continuous lab measurements of solid fraction and temperature during melting allow to test if the flushing parameterization in SAMSIM is also suitable to simulate the evolution of salinity in very thin sea ice during melting. I will compare and discuss the similarities and differences of measured and simulated of melting sea ice.

2 Theory of desalination processes

Sea ice is frozen sea water, so it contains salt. However, the bulk salinity of a melted sea ice sample is usually lower than the salinity of sea water. The reason is that salt cannot be incorporated into the solid ice crystals during freezing. The salt becomes concentrated as highly saline brine in so-called brine pockets in the interior. Sea ice therefore consists basically of a solid part, fresh ice and a liquid part, salty brine and the relation of them can change continuously. Several physical processes were considered to cause desalination in winter and summer. Comparing several laboratory studies and field campaigns, Notz and Worster (2009) found that gravity drainage is the most important process for desalination in winter and flushing and flooding in summer.

2.1 Gravity drainage

Gravity drainage desalinates sea ice during freezing in winter. Cold air cools the water until the freezing temperature is reached and ice formation starts. During the freezing in winter sea ice is at its coldest at the ice-atmosphere interface and grows vertically. Meanwhile the bottom of sea ice is at the freezing temperature of seawater, -1.8 °C. This produces a vertical temperature gradient which goes along with a gradient in brine salinity, as the concentration of brine is determined by the ice temperature (Assur, 1958), see Figure 1. The gradient in brine is unstable because denser brine is located at the cold ice surface and less dense brine at the warmer bottom of the ice. The potential energy of the brine is higher at the ice surface than at the ice bottom. This potential energy difference leads to downwards-draining brine as sea ice is permeable. A convectional overturning process, known as gravity drainage, starts: Some of the upper brine is replaced by sea water from the bottom or lower ice layers. After draining out of the ice, the brine mixes with the underlying seawater and sinks down (Notz and Worster, 2009).

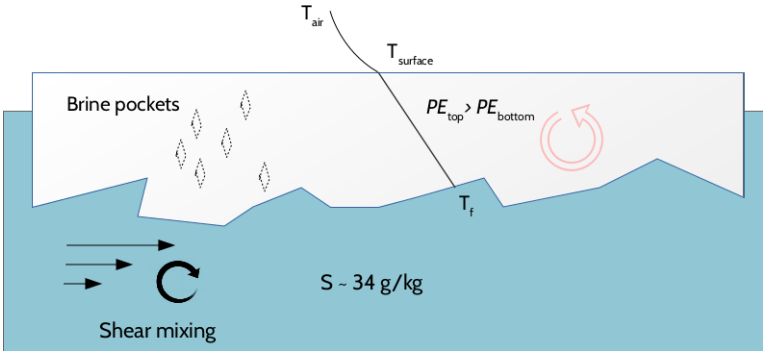

Figure 1. The potential difference between brine and seawater starts a convectional process: Gravity drainage.

2.2 Flushing

Flushing is considered to be the main process of desalination in summer. Higher air temperatures lower the temperature gradient within the ice or even turn it around what stop gravity drainage and increases the permeability. Sea ice starts to melt at the top and melt ponds are created, see Figure 2. They contain relatively fresh melt water which can seep downwards through a brine-channel system in the warm and porous ice and 'washes out' highly saline brine in deeper layers.

Flooding describes the condition that the amount of snow on sea ice becomes so heavy that it pushes the floating sea ice underwater and creates a negative free board. This process is associated with the formation of slush and snow-ice at the snow/ice interface. Flooding is comparable to flushing but with a reversed pressure gradient (Notz and Griewank, 2015). Flooded sea ice is more present in Antarctic because of more snowfall and thinner sea ice than in the Arctic.

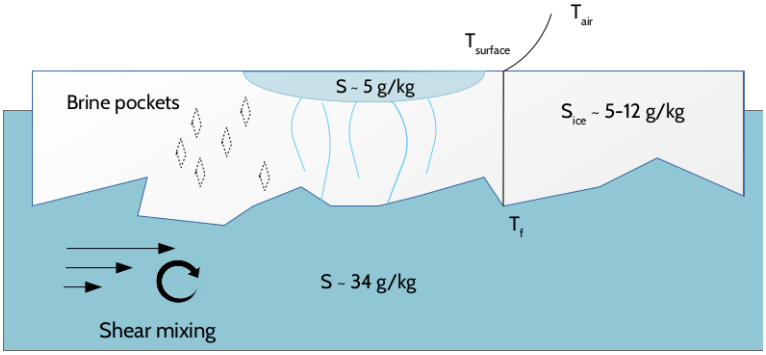

Figure 2. Melt water flushes the ice and 'washes-out' the remained brine.

3 The experimental setup and measuring instruments

To observe the salinity evolution in sea ice during freezing and melting in a laboratory environment, there are several necessary experimental conditions: well-mixed saline water in a closed environment, negative or positive heat fluxes at the water/ice surface and instruments measuring water temperature and salinity, air temperature, and ice temperature and salinity. These conditions and the measurement setup were created in the cooling chamber of the Max Planck Institute for Meteorology (MPI-M) in Hamburg. All experiments described in this work were set up in this chamber. It has a size of about 3 m x 1.2 m and contains a cooling element located outside of the building which provides cold air through air ventilation at one of the short sides of the rectangular room (see Figure 3, right). All the performed experiments are listed in Table 5 with the key boundary conditions: air temperature of the cooling chamber (Cooling), number of measuring devices for ice salinity (number of wire-harps), water salinity (Salinity), water heat input (Heating wires) and if an ice core was taken or not.

3.1 The tanks

Two glass tanks are located in the cooling chamber, simulating a small section of ocean. A small tank can be found in the back of the room. It has a size of 34.6 cm x 34.6 cm and can be filled with water up to 30 cm. This tank has the advantage that it is placed on a metal plate which can cool or warm the water from below and is operated from a thermostat outside of the cooling chamber. Because of its small size it was only used for the calibration of temperature sensors and small experiments to test if measurement instruments are working properly. The larger tank in the room was used for all experimental setups described in this work. It has a size of 196 cm x 66 cm and was filled with water until about 94 cm. Both tanks are isolated by Styrofoam plates to shield the water at the sides. The larger tank is additionally standing on a Styrofoam plate to ensure that the water/ice is just cooled at the surface by the air in the chamber and not at the sides or the bottom of the tank.

3.2 Air conditions

The air in the chamber is cooled by a ventilator at the ceiling at one of the short sides of the room (see Figure 3 right, in the back of the room). Therefore, the air

temperature is not spatially constant in the room. To reduce the air temperature gradient across the tank, the side facing the cooling ventilator is shielded by a plastic plate (see Figure 4, red cover of the left side of the tank). It is meant to provide a relatively homogeneous ice growth across the length of tank. Additionally, a ventilator is placed close to the water surface and mixes air from the un-shielded part of the tank with air from the shielded one (see Figure 4 in the middle, light blue arrows show ventilated air). Nevertheless, there are small differences in temperature and ice thickness observed in the tank during the experiments.

Moreover, the cooling element defrosts every six hours and the air temperatures rise up to 0 °C during this time. For the rest of the time, the room temperature can be set to a certain temperature with a resolution of 1 °C. Nevertheless the air temperature can rise about 4 °C higher than the set value, because the cooling includes a threshold until which temperatures are allowed to rise and the cooling switches on again.

3.3 Heating wires and floating sea ice

To provide a mainly constant mixed water column, two pumps were placed at the short sides of the tank at different heights. They provide a well-mixed water column by creating a vertical overturning circulation in the tank (see Figure 4 blue and red arrow inside the tank). The temperature and the salinity of the water are recorded at two different depths and locations in the tank with CTD's (see Figure 4, illustrated as white cylinders in the middle and on the left-hand side) .

An additional important element of the tank are heating wires at walls of the tank close to the water surface. Five wires cover a height of around 20 cm under the water surface and are meant to prevent the ice from freezing at the walls. This is essential to simulate natural conditions. Freezing ice at the walls prevents the ice from floating as it exerts pressure to the underlying water. The water is forced to rise through brine channels upwards. It was observed that solid ice at the walls can even force the underlying water to flood the ice surface. This process can only be observed in nature when the load of snow on the ice surface becomes as big as it pushes the ice under water and flooding occurs. All experiments were set up without snow cover.

The heating wires are covered by a Teflon foil which creates convection cells of warmed water behind the foil (see Figure 3 left side, grey arrow). This horizontal

tube of warmer water is located directly at the surface and covers around 20 cm water depth. The warm water tube ensures that the ice cannot stick to the walls for ice thicknesses less than 20 cm, which is the operating thickness for salinity measurements. The enclosed water behind the Teflon foil also creates less sharp ice at the sides of the tank. The additional heat fluxes of heating wires and the pumps warm the water slightly but an absolute value is difficult to estimate.

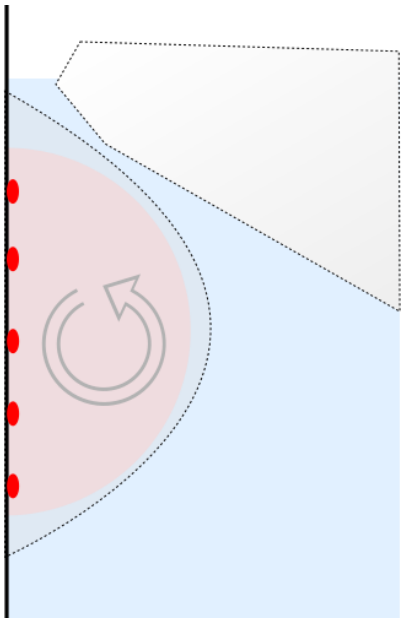

Figure 3. Left: Schematic side view of a tank wall. The Teflon foil covers heating wires (red dots) located close to the water surface and creates a convection cell of warm water. The ice therefore does not freeze to the walls of the tank and is rounded of at its sides. Right: Front view into the cooling chamber.

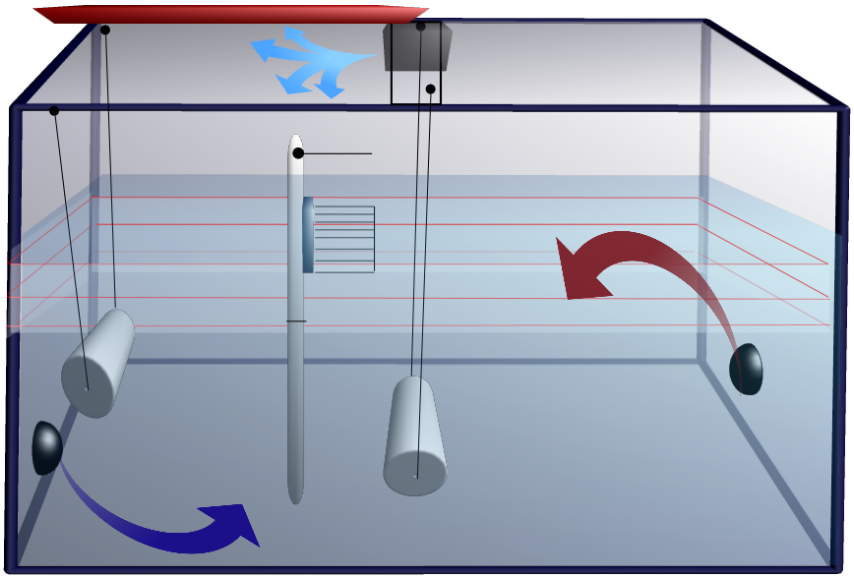

Figure 4. Schematic view of the big tank: Two CTDs, white cylinders, are located at two different depths in the tank. Two pumps create an overturning circulation (red and blue arrow). The wireharp is located in the middle of the tank. The air temperature is measured by a pen-type thermometer close to the water surface. A small ventilator mixes the air (light blue arrows), between the un-shielded and the shielded part of the tank. Heating wires and a Teflon foil close to the water surface prevent the ice from freezing at the walls.

3.4 Measuring instruments

I implemented several measuring instruments in and above the tank to observe the bulk salinity evolution and the boundary conditions of the ice growth. The following measuring instruments were available for the experiments: The air temperature was measured by a pen-type thermometer, water salinity and temperature were measured by two CTDs, (**c**onductivity, **t**emperature, **d**epth measuring device), the ice temperature was measured by small temperature sensors attached to the so-called wireharp, a measuring instrument which can determine the salinity of sea ice in situ.

3.5 The Wireharp

The measurement device hereafter referred as wireharp was first introduced by Notz et al. (2005) and is used for in-situ measurements of solid fraction and temperature in sea ice. The instrument consists of eight parallel wire pairs which have a vertical spatial resolution of 2 cm (shown in Figure 5, left). The instrument can therefore cover an ice thickness of 14 cm. Small temperature sensors, so-called Tsticks are perpendicularly attached to the wire pairs.

The measurement principle of the wireharp is based on the assumption that pure ice is a good electrical insulator and does not allow an electrical flow along the wire pair. The liquid brine in turn allows transport of electrical loading. The measured increase of resistance along the wires is therefore assumed to be proportional to the increase of solid fraction Φ as ice grows (see Figure 5, right). The homogeneity of brine pockets and the solid ice is ensured because the length of wire pairs ($\sim$ 18 cm) is much longer than the typical size of brine pockets ($<$ 1 mm) (NSIDC, 2018a).

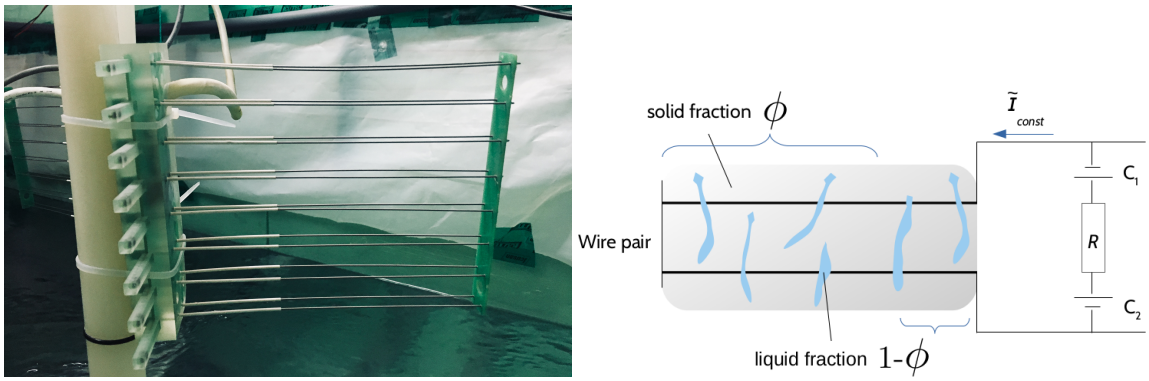

Figure 5. Left: Wireharp attached to a white plastic tube in the tank. Right: schematic view of a wire pair and equivalent circuit diagram. The grey shadow around the wires shows the solid ice and the blue tubes illustrate the liquid brine. Assuming homogeneity of brine and solid ice, the solid fraction Φ and the liquid fraction $1 - \Phi$ of this sea-ice layer can be measured. A constant alternating current is applied to the wires and the voltage drop across the wires determines the resistance of sea ice.

Due to the liquid brine within the solid fresh ice, the current can run across the wire pair. There is a continuous alternating current applied to a wire pair. Across the both wires, the voltage drops due to the electrical insulation of the pure ice crystals. Through the relation $U = R \cdot I$, the resistance R of the medium around the wires can be determined by the applied current I and the voltage drop ΔU, see Figure 5 equivalent circuit diagram on the right. The current I needs to alternate because of the capacitor behavior of the electrical charge of the water/ice around the wires.

For a continuous current, the charge carriers of the medium are sorting along the wire and form a so-called Debye Layer. This layer works as a capacitor which is charging and then prevents the electrical current from flowing. This effect is avoided by applying an alternating current $\tilde{I}$ with a frequency over 10 kHz. By changing the polarization of the electrical current as fast as the charge carriers of the water/ice are not able to sort, the electrical current is constant across the wires. This way

the capacitors C_1 and C_2 can be ignored and only the ohmic resistor R has to be considered, see Figure 5, right.

3.6 Measurement set up

The pen-type thermometer which measures the air temperature is placed about 10 cm above the water surface, close to a wireharp (see for illustration Figure 4). The thermometer and 3 wireharps are attached to white cylindrical plastic tubes which are plugged loosely in plastic bars. These bars are again stucked in plastic tubes which can be mounted at a metal lattice at the bottom of the tank. A wireharp attached to the loose plastic tube is therefore able to move up and down if the expanding ice is moving. Additionally this setup guarantees that the wires of the wireharp stays in one single ice depth during the experiment and are not displaced by deforming ice.

The wireharps are located directly at the water surface at different locations in the middle of the tank. The aim of this measurement setup is to cover inhomogeneities of ice thickness and ice temperatures within the tank. They are caused by a not heterogeneous air fluxes in the cooling chamber due to the fixed location of air ventilation, an insufficient mixing of air within the chamber.

The body of the wireharp is about 1 cm 'higher' than the upper most wire pair, when the instrument is implemented vertically in the water (seen in Figure 5 left, green elongated cuboid). The body contains electronics and need to be covered completely by water to prevent air temperatures from influencing the measurements of the Tsticks. This is why the upper most measurement of solid fraction and ice temperature starts a few centimeters ($\sim$ 2.0 cm) below the water surface for all experiments.

A schematic top view of the measurement set up is shown in Figure 6 and was just slightly varying for the different experiments. That means, the setup of CTDs and the air thermometer stays the same but the location and the number of wireharps are varying. The cooling element of the chamber, which is not part of the scheme is located to the left-hand side of the tank.

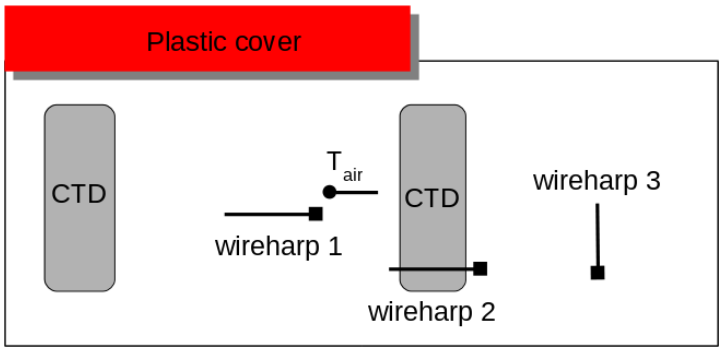

Figure 6. Top view of the tank: The CTD in the middle is located close to the tank bottom. The CTD at the side is located about 35 cm deep. WirearpLocation 1 is installed in the halfshielded part of the tank, wireharp/location 2 in the middle and wireharp/location three is fixed in the un-shielded part of the tank. The air thermometer is mounted above wireharp 1.

3.7 Sensors

For all kind of experiments, it is imperative to know about the uncertainty of the various sensors to interpret the results properly. With the help of uncertainties it is possible to derive absolute errors, calculate error propagation and to interpret the quality of the results.

During all experiments following parameters are measured: air temperature, water and ice temperature, salinity and the electrical resistance of water and ice. The uncertainties are instrument-dependent. The air temperature is measured by a pen-type thermometer which is fabricated by Greisinger measurement technology. It is therefore often referred as Greisinger thermometer in the following. The water temperature in the tank is measured by two different kind of CTD fabricates, a SeaBird CTD and a RBR CTD.

The SeaBird CTD was placed closely to the bottom in the middle of the tank and the RBR CTD in the upper part of the water column the left-hand side of the tank. The eight Tsticks of the wireharp measure the ice temperature in different depths of the forming ice but also measure the water temperature before freezing starts. I calibrated the Tsticks by myself in the cooling chamber what is explained later on. Next to wireharp, I used ice cores to measure the salinity of the sea ice in the large tank. After taking an ice core, it was cut into sections and they melted separately in plastic boxes. The salinity of the melted sections was measured with an hand-hold conductivity measuring instrument, which is named Hach HQ40d Multimeter. The wireharp is measuring the electrical resistance of the surrounding medium either water or ice and its uncertainty is described later on in detail. All sensors are

listed in Table 1 with the respective uncertainty, serial number and if it was known, calibration date.

Sensor	Measured parameters	Uncertainty	Serial number	Calibration date
SeaBird CTD SBE37 SM Microcat	Temperature and Salinity	0.001 $°C$ 0.001 g/kg	37SM55750-7247	July 2015
RBR XR-620 CTD	Temperature and Salinity	n. a.	n. a.	n. a.
Greisinger GTH 3700 PT-100	Temperature	0.03 $°C$	32503104	July 2016
Hach HQ40d Multimeter	Salinity	1 g/kg	081100026390	August 2018

Table 1. List of sensors with respective serial number, uncertainty and calibration date.

3.8 Temperature sensor calibration

As already mentioned the Tsticks of all three wireharps needed to be calibrated in the laboratory environment by myself. The Greisinger thermometer is used as a reference thermometer and was stirred together with the Tsticks of wireharp one in the coolant of the thermostat which is connected with the small tank in the cooling chamber. The liquid oil was cooled down too about -15 °C. During a time of 2.5 hours the constantly circulating coolant slowly warmed up by the room temperature. The Greisinger thermometer was recording constantly every second but each Tstick was just measuring once every 1.5 minutes. The recorded data of the Greisinger thermometer and the Tsticks were then compared for temperatures between -13 °C and 4 °C. A linear function was found for each individual Tstick in the considered temperature range. The Root mean square error (RMSE) of the linear regression for temperatures varies for the 8 sticks of wireharp one between 0.06 °C and 0.1 °C. Therefore a maximum error for the calibrated temperature of the Tsticks is assumed to be 0.1 °C in further error estimations.

The calibration process for wireharp one and three was done similarly. They were placed together with the Greisinger thermometer in a well stirred NaCl concentration in the small tank located in the cooling chamber. The water was mixed by a small pump. The NaCl solution was then slowly cooled down to -15 °C over a time period of eight hours by its thermostat. The temperature data was recorded every four seconds for each Tstick and the Greisinger thermometer was recording constantly every second. The linear regression for wireharp two and three was done the same way as for wireharp 1. The RMSE of temperature calibration for wireharp two and three is about 0.05 °C and hence slightly smaller than from wireharp one. This is probably caused by a slower cooling process and therefore higher resolution of temperature data.

3.9 Error estimation for temperature sensors

During a short experiment which lasted 2.5 hours, the Tsticks of wireharp one, the SeaBird CTD and the RBR CTD and the Greisinger thermometer were placed as close as possible in the big tank which had a temperature of about 2 degrees. The pumps ensured a well mixed water column and the air temperature was held constant in the cooling chamber. This experiment can be seen as a one-point-calibration. From the uncertainty of the sensors, the one-point-calibration and the calibration of Tsticks following error estimations can be derived:

- The temperature measurements of the Seabird CTD are treated as not error-affected
- The temperature difference between the RBR and the Seabird CTD is on a scale of 0.01 °C and is negligible for error estimations
- The temperature difference between both CTDs and the Greisinger thermometer is in the range of the uncertainty of the Greisinger thermometer and will not be considered in error estimations
- The Tsticks have a standard deviation of about 0.02 °C
- The temperature difference between calibrated temperatures from the Tsticks and the Greisinger thermometer is not exceeding the maximum error $\Delta T =$ 0.1°C

4 Theory and error estimation of Bulk salinity calculation

Solid fraction and Bulk salinity

Sea ice is a continuum of solid ice and liquid brine. The solid fraction of sea ice describes the fraction of pure ice and the liquid fraction determines the fraction of the highly saline brine which cannot be incorporated into the ice crystals. The brine stays liquid in small brine pockets because its high salinity lowers its freezing temperature. Before freezing, the solid fraction of seawater is zero but increases with the start of ice growth as sea ice becomes a combination of liquid and solid. The wireharp can determine the solid fraction of growing sea ice around a wire pair because the measured electrical resistance R is assumed to rise proportional to the solid fraction Φ. Based on this assumption the liquid fraction (1-Φ) can be defined as the relation between R and the measured resistance when sea water is still totally liquid R_0 (Notz et al., 2005):

$$1 - \Phi = \frac{R_0}{R}. \tag{1}$$

The salinity of brine S_{br} is defined by the ice temperature because of the relationship between the freezing temperature and salinity of seawater. It can be calculated from the liquidus relationship for seawater from (Assur, 1958):

$$S_{br} = -1.20 - 21.8T - 0.919T^2 - 0.0178T^3, \tag{2}$$

which is valid for ice temperatures from -2 to -20 °. The bulk salinity S_{bulk} is defined as the measured salinity of a melted sample of sea ice. It can be calculated from the measurements of the wireharp by multiplying the brine salinity with the liquid fraction:

$$S_{bulk} = (1 - \Phi) \cdot S_{br} \tag{3}$$

4.1 Choice of R_0

R_0 is the measured value of R of water at the freezing point when its solid fraction is still zero. From this assumption it can be concluded that the value of R_0 for each wire pair can be chosen as R of sea water at the freezing temperature. Practically, At the beginning of ice formation, the ice around the wires is still very inhomogeneous, e.g. ice crystals can form at the body of the wireharp and the wires.

Reasonable values for the bulk salinity can only be calculated after homogeneity of the surrounding ice is ensured and the wire pair is completely enclosed with ice. So this method is not suitable for choosing R_0.

To find a suitable criteria for the choice of R_0, first a Median filter is applied to the time series of R. Otherwise 'Spikes' in the time series, random high values of R, make it impossible to apply a general method to find R_0 within the raw data. To find the start of ice growth at each wire pair, the significant increase of R, I calculate the difference in R after an interval of 25 values. That corresponds roughly to a time interval of 36 minutes. This is done for each wire pair individually, because all wires show slightly different values of R in water at the freezing temperature so have therefore different values of R_0.

R_0 is chosen when the following criteria is fullfilled for the first time:

$$R_0 = R(n);\ \text{for}\ R(n+25) - R(n) > 0.3\ \Omega,$$

n is the time step of the experiment, forward in time. This method is pure arbitrary and variations would lead to slightly different bulk salinities after further calculations. The error in R_0 is suggested as $\Delta\ R_0 = 0.3\ \Omega$ and is demonstrated for a single wire pair in Figure 7, left.

4.2 Procedure of the experiments

To simulate the growth of sea ice, the air temperature in the cooling chamber was set to about -15 °C or -20°C. The freezing was observed until the ice thickness had reached about 16 cm because this is the maximal ice thickness, the wireharp can cover. After all wirepairs measured a significant increase in resistance of the surrounding ice, the air temperature of the room was set to a temperature which was supposed to balance the heat flux from the water and the heating wires. The aim was to create a stable ice thickness and salinity profile. The balancing temperature was estimated by the Stefan's law for ice growth:

$$q_{ice} = -k \cdot \frac{T_f - T_{air}}{h_{ice}}, \tag{4}$$

with $h_{ice} \approx 17$ cm, the heat flux from the heating wires and the water $q \approx 100\ W/m^2$ and $k \approx 2\ W/K \cdot m$. The necessary temperature gradient ($T_f - T_{air}$ can be derived as 8.3 °C . The freezing temperature T_f of the sea water is about -1.8 °C. Therefore, the air temperature was set to -10 °C. The aim of this procedure was to

stabilize the salinity and temperature profile before the melting process starts and took about 2 days.

The melting process was simulated by setting the air temperature to + 5 °C. Due to the positive air temperatures, the ice starts to melt from the top and from the bottom. The aim is to simulate flushing in summer and observe the evolution of solid fraction and bulk salinity profiles.

4.3 Error estimation in bulk salinity

To derive the maximum error for S_{bulk}, different error-affected variables have to be considered. The bulk salinity can be derived by measurements of R, R_0 and T. With Equation 1,2 and 3 the dependence of S_{bulk} on these variables can be formulated as:

$$S_{bulk}(T, R, R_0) = \frac{R_0}{R} \cdot (-1.2 - 21.8 \cdot T - 0.919 \cdot T^2 - 0.0178 \cdot T^3). \tag{5}$$

I assume an error of ± 0.3 Ω for the value of R_0, as explained in subsection 4.1. The value of R is not treated as error affected. The error in temperature measurements is assumed to be ΔT=0.1 $°C$, as described in subsection 3.9. The error of S_{bulk} is then determined by Gaussian error propagation. With the already explained error estimations ΔT=0.1 $°C$, ΔR_0= 0.3 Ω and ΔR= 0 Ω, Δ S_{bulk} can be calculated by:

$$\Delta S_{bulk} = \sqrt{(\frac{\delta S_{bulk}}{\delta T})^2 \cdot \Delta T^2 + (\frac{\delta S_{bulk}}{\delta R_0})^2 \cdot \Delta R_0^2} \tag{6}$$

ΔS_{bulk} strongly depends on the increase in R, because R_0 appears as numerator and R as denominator in Equation 1. Therefore, a strong increase in R as ice growth starts, leads to decreasing values of ΔS_{bulk} for $R >> R_0$. The error in temperature ΔT only affects the calculation of brine salinity. As a consequence, for an increasing R and Φ and the amount of brine becomes smaller. Therefore, ΔT does not strongly influence ΔS_{bulk} for high solid fractions. A representative evolution of S_{bulk} during ice growth for one wire pair is shown in Figure 7, right. The error in bulk salinity sinks from 2.3 g/kg for low solid fractions to 0.3 for high solid fractions. The total error in Bulk salinity for solid fractions higher than 0.8 can therefore assumed as 0.6 g/kg.

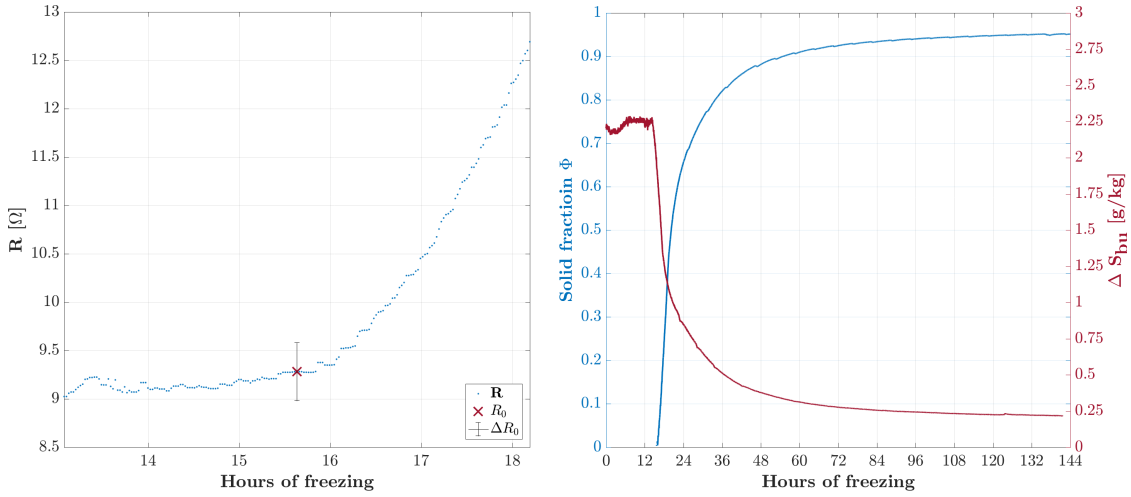

Figure 7. Left: Choice of R_0 and estimated error ΔR_0. Right: Error evolution of S_{bulk} for an strong increase of R.

Ideally, the time when the wire pair shows a significant increase in resistance and the time the temperature stick measures a significant drop, coincide (see therefore Figure 33). This was not found for all experiments. In several experiments it was found that the times of R_0 and the drop in temperature are shifted (see therefore Figure 34). The most obvious explanation for this observation is a wireharp which is not completely horizontally attached. This causes an error in depth of the wire pair itself and in temperature, because the temperature stick does not measure in the same depth as the wire pair.

The depth and the horizontal position of a wire pair cannot be checked or corrected afterwards with the recorded data. But I calculated the error in bulk salinity for a higher ΔT than assumed before, to investigate the influence of a deviating temperature and therefore brine salinity in the calculation of S_{bulk}.

It was found that ΔT dominates the value of ΔS_{bulk} in the beginning of ice growth at a single wire pair because a higher ΔT causes a higher ΔS_{bulk} as it can be seen in Figure 8 for low solid fractions. But after ice formation has started, ΔS_{bulk} sinks to about 0.5 g/kg within 20 hours for all various ΔT. The measured solid fraction has already increased to about 0.8 after this time. This circumstance can be explained as the amount of brine gets significantly small for high solid fractions and therefore the uncertainty in temperature becomes less important. So it can be assumed that ΔS_{bulk} is about 0.5 and the total error of $S_{bulk} = 1$ g/kg for solid fractions greater or equal 0.8.

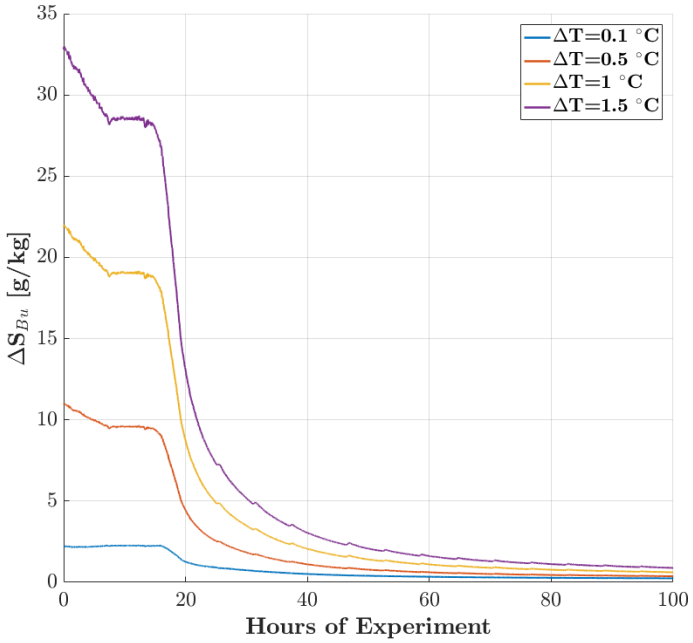

Figure 8. Evolution of ΔS_{bulk} in an ice depth of 2 cm for ΔT = 0.1, 0.5, 1 and 1.5 °C.

4.4 Error estimation for melting

During melting, the wire pairs measure a significant decrease in resistance due to warming and melting ice. This leads to an increasing $\Delta\ S_{bulk}$ in contrast to the freezing process. From the calculated errors by Equation 3, I find that $\Delta\ S_{bulk}$ increases up to 2.3 g/kg for decreasing solid fractions smaller or equal 0.6. Therefore the calculated bulk salinity during melting can not be treated as highly reliable for small solid fractions. I rather consider the temporal trend in bulk salinity for an advanced melting and an increasing liquid fraction.

4.5 Salt budget

To evaluate the quality of salinity measurements, I did a simple salt budget calculation: I multiply the calculated salinity in a single ice layer $S_{bu,ice}$ with its thickness h_{ice} and sum it with the respective water depth h_{water} and salinity $S_{bu,water}$ of the underlying water. For a closed salt budget this equals the salinity multiplied with the water depth S_{total} and h_{total} at the start of an experiment when the tank is totally ice-free. The following equation is solved for S_{total} at each time k when a new wire pair is enclosed by ice to ensure the optimal knowledge about the current ice thickness, whereas n is a single ice layer :

$$\sum_{n=1}^{k} h_{ice}(n) \cdot S_{bu,ice}(n) + h_{water}(k) \cdot S_{bu,water}(k) = S_{total} \cdot h_{total} \tag{7}$$

I calculate S_{total} for eight ice thicknesses and can therefore asses if the quality of the calculated salinities is depended of the ice thickness. An error in ice thickness was estimated as $\Delta\ h_{ice}$= 1 cm, because of roughness at the ice bottom and misalignment of the wireharp. The inhomogeneity in ice thickness across the tank is not covered by this estimation, the assumed error would be too optimistic. ΔS_{total} can be calculated by the uncertainties of Δh_{ice}= 0.01 m, Δh_{water}= 0.01 m and ΔS_{bulk} derived from Equation 6 as:

$$\Delta S_{total} = \sqrt{(\frac{S_{bu,water}}{h_{total}})^2 \cdot \Delta h_{ice}^2 + (\frac{S_{bu,ice}}{h_{total}})^2 \cdot \Delta h_{water}^2 + (\frac{h_{ice}}{h_{total}})^2 \cdot \Delta S_{bu,ice}^2} \quad (8)$$

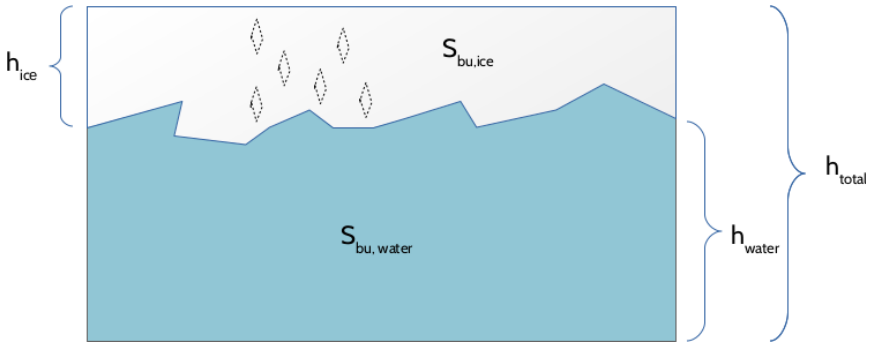

Figure 9. Schematic view of variables used in Equation 7.

5 The 1-D sea-ice model SAMSIM

One way to use the measured profiles of salinity and solid fraction for a better understanding of desalination is to investigate, how far a model, including the respective physical processes, can reproduce the measurements. For this purpose, I use a 1-D thermodynamic Semi-Adaptive Multi-phase Sea-Ice Model, called SAMSIM, developed by Griewank and Notz (2013). The main aim of the model study is to investigate how well the physical description of desalination processes in SAMSIM can simulate the salinity and solid fraction measurements during freezing and melting.

5.1 Model description

SAMSIM was developed to understand how gravity drainage affects the thermodynamics of sea ice. Its thermodynamic core is based on the mushy-layer equations of sea-ice (Feltham et al., 2006) and was extended by a gas phase, gravity drainage, flushing and flooding. SAMSIM is semiadaptive because it does not contain a prescribed ice-ocean front but the solid fraction in every layer increases for a constant ice thickness. This allows a detailed description of brine dynamics because it describes sea ice as a continuum of a solid and liquid part. Furthermore SAMSIM contains vertically and horizontally homogeneous layers whereby each single layer is defined by four core variables: absolute salinity, absolute enthalpy, mass, and thickness. A full description of the thermodynamic core of SAMSIM is described in Griewank (2013).

5.2 Gravity drainage parameterization

Gravity drainage was found to be the main process of desalination during freezing (Notz and Worster, 2009). As it is a convective process, it is a three-dimensional process and can just be parameterized in SAMSIM which is a 1-D model. A convective parameterization simulates brine movement, based on a few basic assumptions and a simple parameterization computes the salinity evolution. The strength and onset of gravity drainage is referred to a Rayleigh number Ra which describes the ratio of driving buoyancy to the thermal diffusion and viscous resistance in a porous medium. SAMSIM defines the Rayleigh number for a single layer i as:

$$Ra^i = \frac{g \Delta \rho^i \tilde{\Pi}^i h^i}{\kappa \mu}, \tag{9}$$

with the standard gravity g, the density difference between the brine of layer i and the lowest layer $\Delta\rho^i$, the distance from the layer i to the ocean h^i, the thermal diffusivity κ. With some assumptions, Ra can be used to define the onset and strength of gravity drainage. These assumptions include that there is a critical value of the Rayleigh number. For values which exceed these critical Rayleigh number R_{crit}, so that the potential energy overcomes thermal diffusivity and friction, brine leaves the respective layer through a channel system and get resolved in the underlying water. This brine is replaced by water as it is a convectional process. The amount of brine which leaves a certain layer is proportional to the difference Ra of the respective layer and R_{crit}.

The uncertainty of this number is high because the assumed permeability is not very uniform across varying studies. The way SAMSIM is defining Rayleigh numbers is to distinguish between the whole vertical sea ice profile and the convectional flow between a single layer and the underlying water. The complete definition of the Rayleigh number and how it is implemented in SAMSIM can be found in Griewank and Notz (2013 and 2015).

5.3 Flushing parameterization

Besides gravity drainage, Griewank and Notz (2015) introduced a flooding and flushing parameterization which can be used to simulate the salinity evolution in sea ice during melting. Until now, there are just a few flushing parameterizations implemented for a full thermodynamic sea-ice ice model (Vancoppenolle et al., 2006 and Griewank and Notz, 2013), SAMSIM is one of them. Vancoppenolle et al. (2007) could reproduce field measurements of salinity by assuming that after sea ice has reached a certain permeability, a fraction of melt water flows vertically through brine channels in the underlying ocean. Additionally to the vertical component of flushing, SAMSIM includes a horizontal component of brine movement which was found to occur in the upper layers of sea ice by Eicken et al (2002): The brine moves horizontally until it reaches a crack through which it can flow downwards into the ocean or even forms new ice at layers where it can freeze again due to its low salinity. The aim of SAMSIM's flushing parameterization is, to implement a physically consistent system including vertical and horizontal brine fluxes. A full description and its implementation in SAMSIM are described in Griewank and Notz (2015).

5.4 Forcing of SAMSIM

SAMSIM offers different ways to implement heat fluxes causing the growth of sea ice. One way is to calculate the heat flux between air and water by assuming a proportionality of the difference between the temperature in 2 meters above the ice and the ice-surface temperature. This temperature forcing was chosen for the simulation of melting. For the freezing process, the best way to simulate the observed ice growth was found to force SAMSIM with the time-corresponding temperatures of the ice surface, referred hereafter as T_{top}.

The ice temperature is measured by the temperature sensors of the wireharp with a 2 cm vertical-spacing whereby the first sensor is implemented 2 cm below the water surface. I assume a perfect linear temperature profile within the ice and calculate T_{top} by doing a linear regression whenever a new temperature sensor registered cooler temperatures than the freezing temperature, see Figure 10, left. T_{top} was than interpolated in time so that simulated time matches the experimental time. The time step in SAMSIM is one second but the output was chosen as only one per hour.

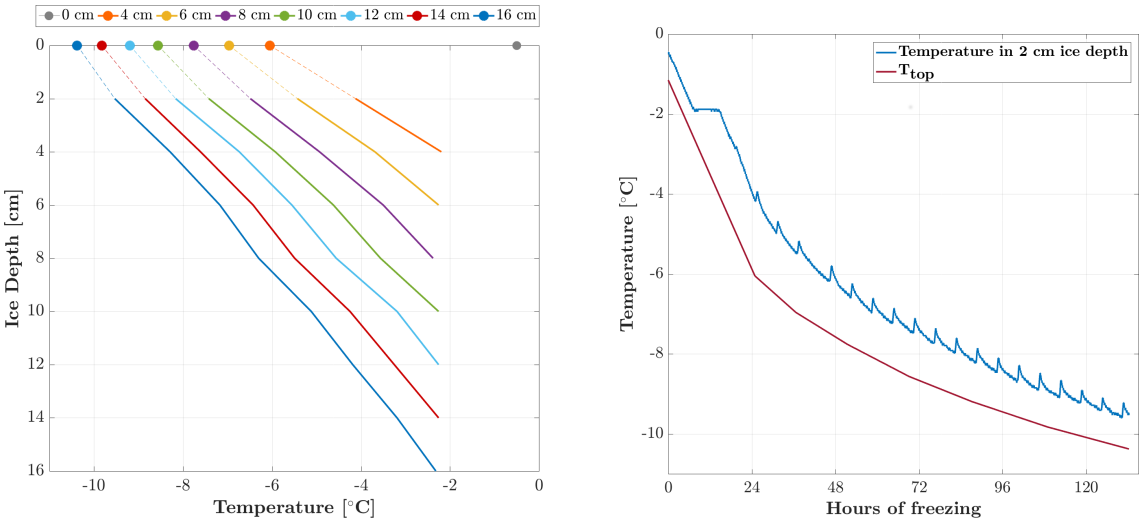

Figure 10. Left: Profiles of ice temperature, when ice has reached a deeper temperature sensor. The dots show T_{top}, derived by a linear regression. The grey dot is a start temperature, when no sea ice is existent. Right: Evolution of the temperature in 2 cm depth for a freezing process and the derived temperature at the ice surface, T_{top}.

T_{top} can just be calculated for ice thicknesses greater equal 4 cm, because for 2-cm-thick ice there is just a single temperature measurement and a linear regression is not possible. T_{top}, before ice growth starts (grey dot in Figure 10, left) was set to

a certain temperature. This temperature was chosen by comparing the times of an ice thickness of 2 cm in the experiment and a simulated ice thickness of 2 cm in SAMSIM. T_{top} was then chosen when the times of 2-cm-thick ice in coincide best in the experiment and in the simulation. For the temporal evolution of ice thickness, the best agreement for experiment and simulation was found by choosing a certain heat flux from the water.

6 Which temporal evolution of Bulk salinity can be observed with the wireharp during freezing?

In the following chapter, I will document the data processing a freezing experiment (referred to as **Exp_20_1**). The measured profiles of solid fraction and bulk salinity will answer the question which profiles of solid fraction and bulk salinity evolve in the growing artificial sea ice and if the results are reliable and comparable to alternative measurement methods, like ice cores.

6.1 Boundary conditions

To initialize ice growth, the cooling element of the cooling chamber was set to -20 °C. The actual air temperature close to the ice surface either varied mostly between -16 ± 0.01 °C and -20 ± 0.01 °C (see Figure 11, left). The temperature variations are caused by the operation of the cooling element (explained in subsection 3.2). The sub-zero air temperatures provide a cooling of the water surface. The positive heat input by the heating wires close to the water surface was set to 100 Watt to prevent the ice from freezing at the walls.

The temporal evolution of the water temperature and salinity during the freezing process is shown in Figure 11, right. The water salinity increased from about 33.1 ± 0.001 g/kg before ice growth to 39 ± 0.001 g/kg when the ice had reached a thickness of about 16 cm. The water temperature increased from about -1.9 ± 0.001°C to -2.2 ± 0.001 °C. Both CTDs show nearly the same values (deviations smaller than 0.01 °C), therefore I just show the measurements from the seabird CTD implemented close to the bottom in the middle of the tank.

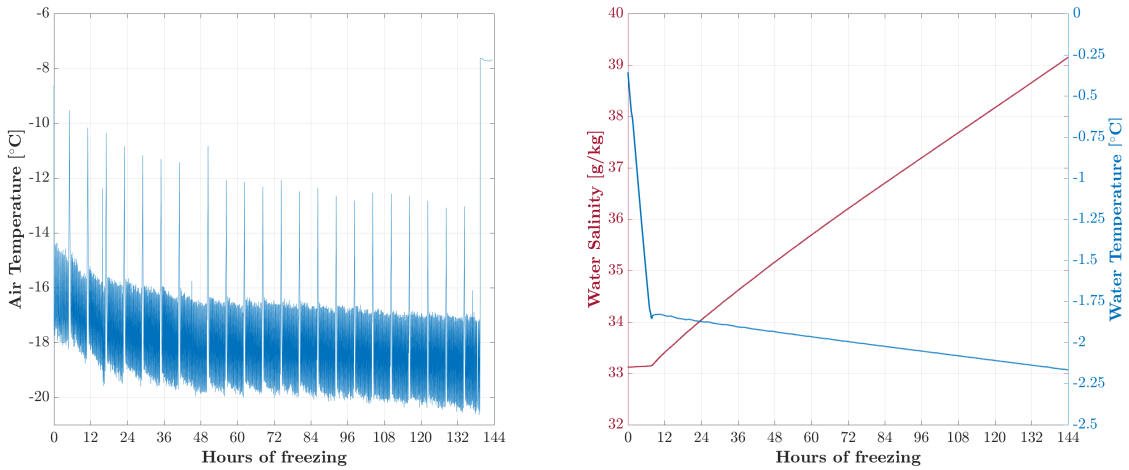

Figure 11. Left: Temporal evolution of air temperature during the freezing process. The variations are caused by the operation of the cooling element. Right: CTD measurements of water salinity and water temperature during ice groth.

6.2 Temperature profiles

The wireharp was implemented in the left part of the tank (see Figure 6, wireharp/location 1) about 2 cm below the water surface. The vertical resolution of temperature sensors and wire pairs is 2 cm, therefore the measurements can cover 16 cm of ice. The temporal evolution of calibrated temperatures is shown in Figure 12, the color legend of the graphs can be understood as the ice depths of Tsticks. The ice grew to about 2 cm in about 15 hours of recording. The freezing temperature of the water was already reached after 8 hours and can be identified as the end of a strong decrease in temperature. The times when ice growth reached greater depths is listed in Table 2.

The temperature evolution shows the expected decrease after ice encloses a deeper temperature sensor. The three upper most Tsticks 'feel' the air temperature variations caused by the cooling element of the chamber (compare to Figure 11, left). The freezing temperature of the water sinks over time because the salinity of the water increases due to released brine. This slow increase of water temperature agrees well with the measurements of the CTD (see also Figure 11, right). This indicates a well mixed water column because the temperature measurements close to the bottom of the tank agree with the temperatures directly under the ice. The temperature measurements also show a nearly linear temperature gradient from the cold surface to the warm ice bottom. The ice becomes colder in all depths when time progresses. This indicates that the temporal increasing solid fraction comes along with brine

getting more concentrated. When the ice has grown about 16 cm, the uppper most temperature sensor in 2 cm depth measures about 9.5 ± 0.1 °C and the ice bottom is about 2.2 ± 0.1 °C.

Ice thickness [cm]	Time [h]
2	7
4	16
6	27
8	41
10	59
12	79
14	99
16	120

Table 2. Time in hours, after which the water has reached the freezing temperature. Ice thickness is referred to the depth of wire pairs.

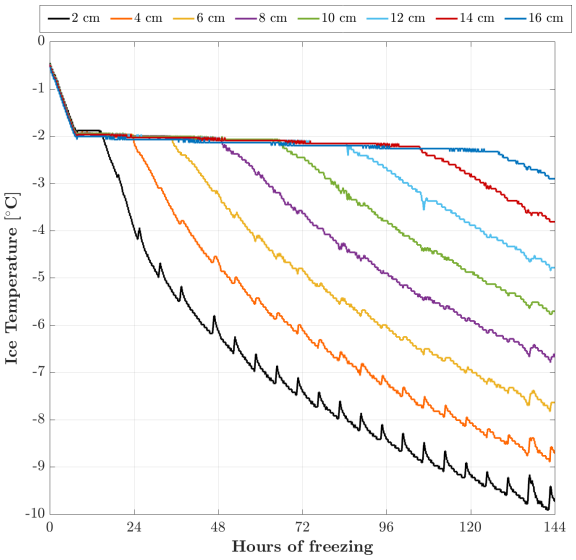

Figure 12. Temperature evolution of every single Tstick. The colors represent implementation/ice depths.

6.3 Resistance measurements and solid fraction

The wireharp measures the electrical resistance R of the ice surrounding a wire pair. The recorded data of R of **Exp_20_1** is shown in Figure 13, left. A significant increase in R indicates that ice starts to form around a wire pair. This special time and the concerning value of R, called R_0 and was found by a self-selected method, described in subsection 4.1. The times when R is increasing suddenly, coincide well with the times for the start of ice growth found in the temperature measurements (compare to times of Table 2). Hence, the ice thickness can be identified by both measured parameters for this special freezing experiment. The wire pairs in the respective ice depths show a chronological ice growth from 2 cm to 16 cm. The measured R also feels the variability in air temperature what can be seen as small variations in ice depths of 2 cm and 4 cm.

From R and the parameter R_0, the solid fraction Φ can be derived by Equation 1. The first values of Φ after ice-growth starts (ca. 1 h after a significant increase in R

for every wire pair) has to be ignored, see subsection 3.5. Φ increases from 0 (liquid water) and is approaching to 1 (pure ice) during freezing. The calculated values for Φ show the expected increase over time. After a certain time the solid-fraction increase stagnates for every wire pair. When the ice thickness has reached 16 cm, Φ is very uniform in the upper most 10 cm (about 0.94), 0.9 in 12 cm and 0.85 in 14 cm ice depth.

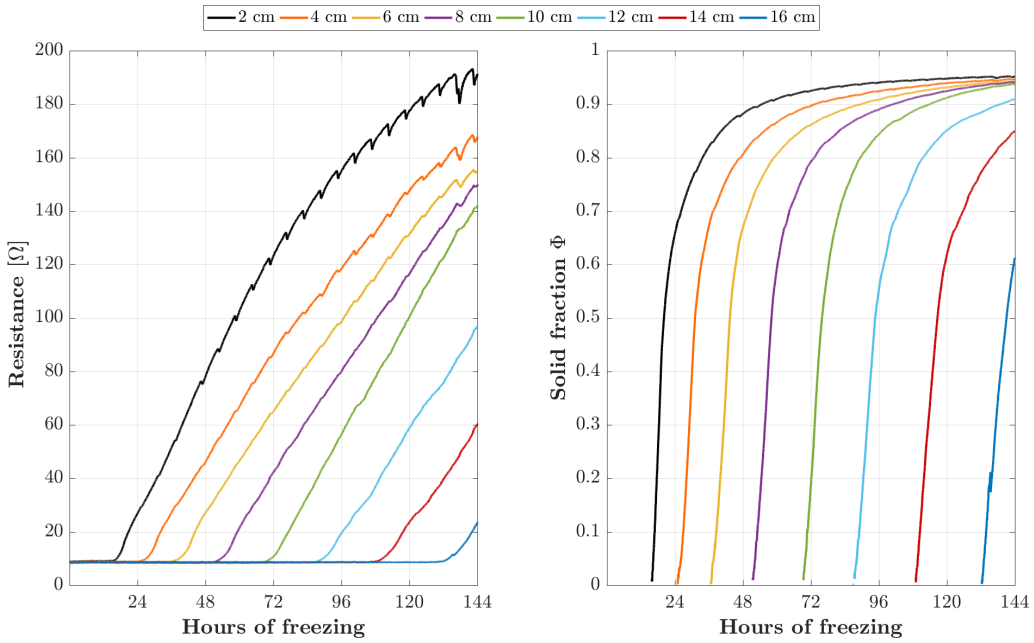

Figure 13. Temporal evolution of resistance measurements (left) and solid fraction (right) during freezing. Time in hours responds to the data-recording and the colors show ice depths.

6.4 Bulk salinity and Salt budget

The measured ice temperatures determine the brine salinity, S_{br} by Equation 2. From S_{br} and the liquid fraction (1-Φ), the temporal evolution of the bulk salinity S_{bulk} can be calculated by Equation 3. The profiles in Figure 14 show the bulk salinity in all ice depths at the time when ice growth has reached a deeper wire pair, hence the colors represent the salinity profile of ice with a certain thickness. The black crosses show the current salinity of the underlying water which is assumed to equal the salinity of the newly forming ice at the ice bottom. The dots in Figure 14 show the calculated values of bulk salinity in the respective ice depths. They are connected linearly because the salinity profile in sea ice is assumed to be continuous.

The profiles illustrate that the bulk salinity over the whole ice column is lower than the salinity of the underlying water. The bulk salinity is decreasing in all ice depths for increasing ice thickness, what can be understood as a decrease in time. The

strongest decrease can be found in 2 cm depth until the ice thickness has increased to 14 cm (red profile). The deeper ice layers desalinate chronology until the bulk salinity is relatively equal in all ice depths from 2 cm to 10 cm for an ice thickness of 14 cm. There is a big jump from a high to a low salinity between the greatest ice depth of a profile and 2 cm depth above. This jump becomes stronger for increasing ice thicknesses because the water salinity increases over time. When an ice thickness of 14 cm is reached, the bulk salinity from 2 cm to 10 cm depth is approximately equal if about 8 ± 0.6 g/kg. The salinity in 12 cm ice depth is about 14 ± 0.6 g/kg and the salinity in 14 cm depth equals the salinity of the water, 37.5 g/kg. For an ice thickness of 16 cm, the salinity profile changes slightly. The lowest bulk salinity can be found in 10 cm depth (about 6.5 ± 0.6 g/kg) and increases slightly from 10 cm upwards to about 7 ± 0.6 g/kg and increases towards the ice bottom. This 'buckling' of the salinity profile continues slowly for later times (later shown in subsection 4.2).

In general it can be said, that the salinity profile is not C-shaped as it was found in measurements of Arctic ice cores of thin ice, up to 30 cm thick (Kovacs, 1996). It is rather formed as half C-shaped, because a low salinity in the interior is followed by a strong increase in salinity in the lowest-most 4 cm of all thickness profiles but the increase in salinity at the ice surface is missing. On the other hand, the measurements start in 2 cm ice depth and the salinity of the ice below remains unknown. I will return to measured salinity profiles in greater detail in subsection 7.2.

6.5 Salt budget calculation

To evaluate the measurements of the wireharp, I did a simple calculation for the sum of the bulk salinity S_{bulk} and the water, S_{total} by Equation 7. The salinity budget was calculated for times when ice growth reached a deeper wire pair to get the best assumption of the current ice thickness. The results of the budget calculation are listed in Table 3 for the respective ice thicknesses. The salinity of the water before ice growth has started was measured as 33.07 g/kg by the CTD. The calculated values of S_{total} converge slightly to the original water salinity as the ice becomes thicker. Generally S_{total} is about 1 g/kg higher than the original salinity of the water. The absolute error was calculated by Equation 8 and is getting smaller for increasing ice depths. This behavior seems reasonable because the uncertainty caused by the not-known salinity of the upper most 2 cm of ice, becomes less important for greater a ice thickness. Additionally, the sum of $\Delta\ S_{bulk}$ of the different ice depths becomes

smaller for an increasing solid fraction and the ratio Δ h_{ice}/h_{total} becomes smaller which also lowers the error. Due to the small difference between the water salinity and S_{total}, the budget calculation contributes to the reliability of the bulk salinity derived by the measurements of the wireharp.

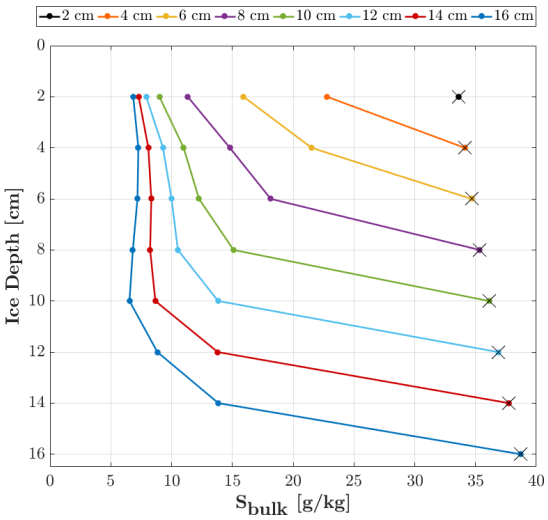

Figure 14. Profiles of bulk salinity for increasing an ice thickness (colors). The crosses in the respective greatest ice depth indicate the water salinity assumed as the salinity of newly forming ice.

Ice thickness [cm]	S_{total} [g/kg]
2	33.70 ± 3.36
4	34.04 ± 2.85
6	34.05 ± 2.41
8	34.03 ± 2.00
10	33.99 ± 1.69
12	33.95 ± 1.50
14	33.95 ± 1.36
16	33.98 ± 1.26

Table 3. Table of S_{total} the sum of ice and water salinity for increasing ice thicknesses. The values and their error are calculated by Equation 7 and Equation 8.

6.6 Ice-core measurements of bulk salinity

Another way to validate the salinity measurements by the wireharp is the comparison with ice-core measurements. During the experiment **Exp_20_1**, an ice core was taken close the wireharp after about 160 hours of recording (see Figure 35), before the temperature in the cooling chamber was set from -20 °C to -10 °C. As an ice core often decomposes already before cutting it into pieces, the sections of the cores are not uniform. So the length of the different sections differs from 2.5 cm to 4 cm. The measured bulk salinity of the different melted sections are shown as red vertical bars in Figure 15, respective their length. The bulk salinites of the wireharp at this time are shown as blue crosses.

The core sections represent S_{bulk} of different depths and can not be compared one-to-one with the measurements of the wireharp due to the different spacing. The wireharp observes that the bulk salinity has increased in the upper most 6 cm during the elapsed 15 hours after the ice has reached a thickness of 16 cm (compare to Figure 14). The tiny decrease in salinity which could be seen in 8 cm and 10 cm in

has continued and leads to a bulk salinity of 5.3 ± 0.6 g/kg in 10 cm and 5.7 ± 0.6 g/kg in 8 cm depth. The salinity in the upper most 6 cm is about 6.8 ± 0.6 g/kg. The salinity of the core sections in comparison to the respective depths of wireharp measurements is in a very good agreement for the 3 'interior' sections of the core, from about 6 cm to 12 cm ice depth. The inner core sections are just 1 to 2 g/kg higher than the measured bulk salinity of the wireharp, what can be treated as a good agreement as the uncertainty of the measurement instrument which was used to measure the salinity of the melted ice core sections, is about 1 g/kg.

The bulk salinity of the upper most core section is much higher than the wireharp's measurement in 2 cm and 4 cm ice depth. That is very likely due to the fact that the salinity of the 2 cm is unknown. The lowest ice core section shows a relatively low bulk salinity of about 8.5 ± 1 g/kg in contrast to the wireharps's bulk salinity of about 15 ± 0.6 in 16 cm depth. This might be caused by brine loss at the bottom edge during taking the core. Concerning these attempts of explanation I would interpret the comparison of the measured bulk salinity by the wireharp and the core measurements as another confirmation for the reliability of the measurements of the wireharp.

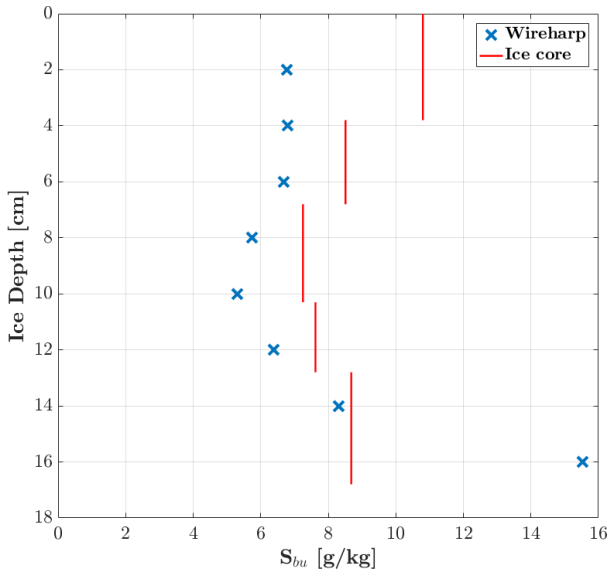

Figure 15. Comparison between ice-core-section salinities and calculated bulk salinities of the wireharp in 2 cm vertical spacing, after 160 hours of recording the freezing process.

7 How well can SAMSIM simulate the measured profiles of temperature, solid fraction and bulk salinity?

The freezing process of **Exp_20_1** was simulated with SAMSIM to investigate the agreement of my lab measurements and a model which includes the respecting physics of desalination during freezing. To achieve a suitable comparison, I forced the model by the top temperatures of the ice, determined by the measured temperature profiles for increasing ice thicknesses (explained in subsection 5.4). SAMSIM assumes a perfect linear temperature profile across the whole thickness, where the coldest temperature can be found at the ice surface. The ice-bottom temperature is the freezing temperature of the water below, which depends on the current water salinity.

I found T_{top} for the start of simulation by choosing a value which provides the best temporal agreement between measured and simulated ice thicknesses of 2 cm and 4 cm. This was necessary because T_{top} can just be calculated for ice thicknesses ≥ 4 cm. For the further temporal agreement of measured and simulated ice thicknesses, the heat flux of the water was set to a value which showed the best agreement for thickness and temperature evolution.

To answer the question, how well SAMSIM can simulate the measured profiles, I decided to compare profiles of equal ice thicknesses (colored profiles in Figure 16 and Figure 17). That means, I compare temperature, bulk salinity and solid fraction profiles for the times, when a deeper temperature sensor shows a significant decrease in temperature below the freezing temperature, with the respective values from SAMSIM. I justify this decision by the fact that I just know about the exact ice thickness in the lab when a new sensor is reached and that the simulated and measured ice thickness agrees very well in time. A reason for comparing equal times would have been that the time simulated in the model elapsed as fast as in the measurements because T_{top} was respectively temporal interpolated. This could cause a better agreement of temperatures in 2 cm depth but I would lose information of the current ice thicknesses in the lab measurements and therefore, I decided to compare laboratory and simulated sea ice of the same thickness.

7.1 Ice thickness and Ice temperature

The layer thickness in SAMSIM was set to 0.02 cm, therefore the simulated profiles are much higher resolved in depth than the lab measurements which are only 2 cm vertically spaced. As already mentioned the measured ice thicknesses in the lab agree very well with the simulated thickness after adapting the heat flux and T_{top} in the beginning of the experiment (see Figure 16, left). The deviation of equal ice thicknesses does not exceed 2 hours for **Exp_20_1**. The temperature profiles for increasing ice thicknesses agree very well with the modelled profiles (see Figure 16, right. Colors represent the current ice thickness). The difference between the measured and the modelled profiles have a maximal absolute deviation of 0.1 °C except the temperatures at the ice bottom. This small difference does not even exceed the error in measured temperature, derived from the sensor calibration. The simulated temperature at the ice bottom is increasingly slightly higher for increasing ice thicknesses than the measured bottom temperatures.

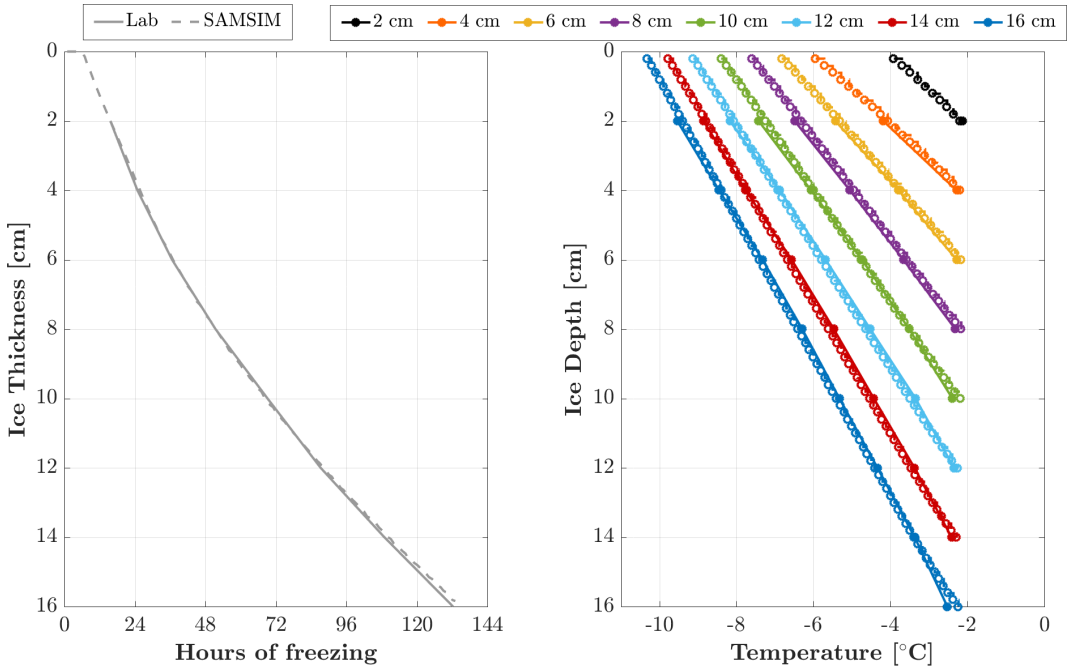

Figure 16. Temporal evolution ice thickness (left) and temperature profiles (right) for increasing ice thicknesses in different colors. The lab measurements are shown as filled circles, connected by a solid line. The simulated temperatures are shown as blank circles, connected by a dashed line.

7.2 Bulk salinity and solid fraction

As a first result of the comparison between the measured and simulated solid fraction and bulk salinity, it can be said that the shapes of profiles are very similar for all ice

thicknesses (see Figure 17, left). For the uppermost 2 cm ice, there are no measurements provided by the wireharp. SAMSIM shows a strong decrease in salinity of 25 g/kg and 30 g/kg at the ice/air interface to a salinity of about 10 g/kg in 2 cm ice depth. These high values at the surface are caused by the implementation of gravity drainage in SAMSIM which is further described later on. Furthermore the simulated and measured profiles mostly differ in absolute values and the agreement becomes less good for greater depths. The greatest depth of each thickness profile coincides well as the salinity of newly forming ice equals the water salinity in lab measurements and in SAMSIM. However, it can be seen that this agreement becomes less precise for the bulk salinity in the lowest layer for greater ice thicknesses. SAMSIM seems to underestimate the water salinity because this trend can not be found in such a strong way in the comparison between measured and simulated solid fraction (see Figure 17, right). This could be caused by a lower measured bulk salinity over the whole ice thickness than the simulated bulk salinity for an ice thickness greater equal 10 cm. That explains why SAMSIM underestimates the water salinity, and therefore the salinity of newly forming ice, due to a higher simulated salinity content in the ice.

The measured bulk salinity of 16-cm-thick ice is about 4 $\pm$ 0.6 g/kg to 5 $\pm$ 0.6 g/kg lower than the simulated bulk salinity for all depths except the ice bottom. This is a relatively high deviation if I calculated an absolute error in the measured bulk salinity of 0.6 g/kg. At low solid fractions, the error is relatively high, about 2.3 g/kg but it can be neglected in the comparison of profiles because the solid fraction increases as fast as that it is already about 0.8, 2 cm above the ice bottom.

The absolute values of measured and simulated solid fractions seem to agree better than the absolute bulk salinity even if the measured solid fraction is slightly higher than the simulated solid fraction. It is caused by the fact that a small deviation in solid fraction leads to a relatively high deviation in bulk salinity.

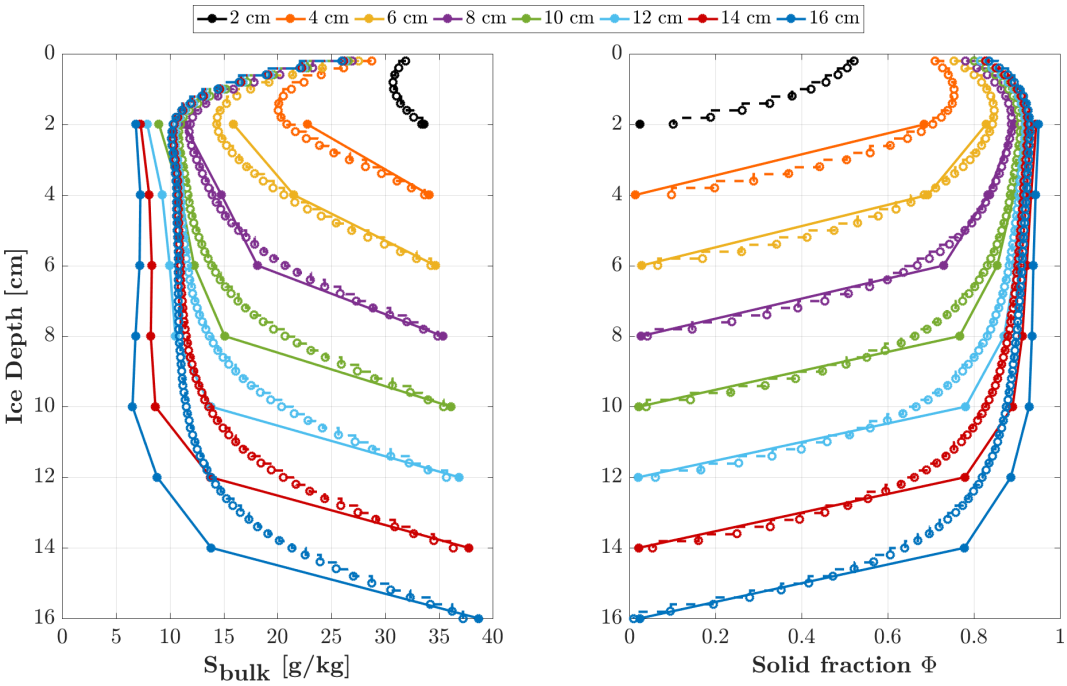

Figure 17. Profiles of bulk salinity and solid fraction for increasing ice thicknesses in different colors. The filled circles are the lab measurements. The dashed lines/ blank circles are the simulated profiles.

SAMSIM simulates the bulk salinity and the solid fraction in respect to brine fluxes which result from a gravity drainage parameterization, introduced in Griewank and Notz (2013). The parameterization is based on the assumption that the Rayleigh number (Equation 9) describes the onset and strength of gravity drainage which was found to be the only valid desalination process during freezing (Notz and Worster, 2009).

With the use of ice temperature, volume fraction and brine salinity of all active layers from 1 to n, SAMSIM calculates the Rayleigh number of each layer i (see for explanation subsection 5.2). If $Ra^i > Ra_{crit}$, a critical Rayleigh number, the layer i is considered as unstable and the mass of brine that flows from layer i into the ocean in a time step of length dt is calculated by:

$$br^i_{\downarrow} = \alpha(R^i - R_{crit})\Delta z^i \cdot dt.$$

Further implemented brine dynamics of SAMSIM are explained in Griewank and Notz (2013). However, this parameterization only includes two free parameters: R_{crit} and α. These both values were tuned with the help of lab measurements from Notz et al. (2005) who implemented a wireharp beneath a cooling plate and measured the solid fraction and temperature during freezing (shown in Figure 18).

The so-called 'C-profiles' of bulk salinity in sea ice (high salinites at the surface of the ice, low values in the interior and increasing values towards the bottom) which SAMSIM simulates, are caused by the definition of the Rayleigh number. As it was explained before, gravity drainage and the respective brine fluxes into the underlying water are supposed to set on when R_{crit} is reached. For very thin sea ice, a critical value cannot be reached, because the difference between the potential energy of brine (see Equation 9) and seawater is not high enough. This causes the simulated high salinity in the top layers. This so-called 'delay in onset of gravity drainage' was found to be consistent with CTD measurements by Wettlaufer et al (2000) in the Antarctic ocean but is not consistent across different studies (Notz and Worster, 2008). In my measurements, this delay cannot be observed for ice depths greater equal 2 cm ice depth. Furthermore, the freezing temperature at the water surface is reached during the cooling process after about 7.2 hours (see Figure 12) and the water salinity started to increase after about 7.5/8 hours (see Figure 11, right). Considering that the CTD was installed relatively close to the tank bottom, I would conclude that this delay in onset of desalination cannot be found in CTD measurements for this experiment.

Furthermore, I would interpret the offset in salinity at the ice bottom of the different profiles (see Figure 17, left) caused by the generally higher salt content of the whole ice column in SAMSIM in contrast to my measurements. SAMSIM has implemented a salt-budget calculation, which ensures that the salinity of the underlying water volume increases proportional to the brine what is drained out of the ice. As the simulated salt content in the ice is generally higher, a lower water salinity will be calculated by the model and the newly forming ice has therefore a slightly lower salinity than the measured salinities.

As mentioned before, the gravity drainage parameterization of SAMSIM was tuned by lab measurements of solid fraction and temperature measurements (shown in Figure 18). These experiments were conducted under following boundary conditions: There was no free ice surface due to a cooling plate on the top of the water. The temperature of the plate was switched from -5 °C to -10 °C every 12 h. The experiment was conducted twice under the same temperature conditions. My experiments were conducted with a free surface and the air temperature was held relatively constant during the whole time. The Figure 18 shows the profile of bulk salinity across the ice column for 24 h, 48 h and 72 hours of freezing. The profiles show a higher

bulk salinity at the ice top and the ice bottom. A low bulk salinity can be found in the interior, but the salinity is not as homogeneous in the interior as it was found in my measurements.

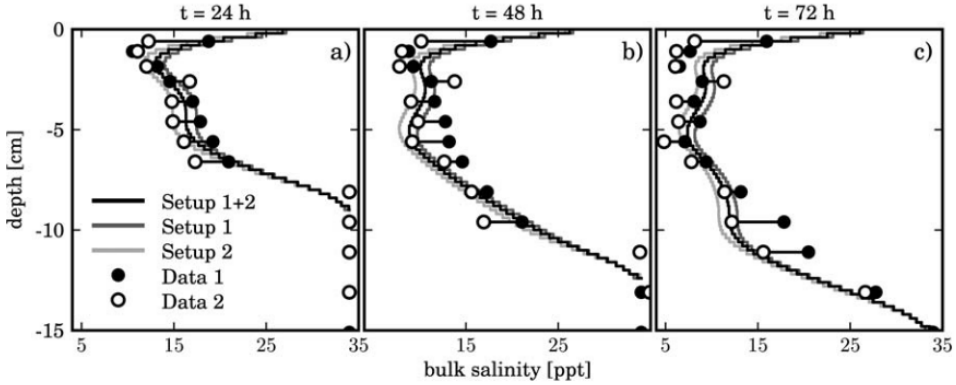

Figure 18. Lab measurements from Notz (2005) of bulk salinity profiles after 24 h, 48 h and 72 h of freezing. Setup 1 and 2 are two experiments for similar boundary conditions (Setup 1 and 2: black and white dots) and the respectively fitted profiles of SAMSIM (grey and black lines). Adopted from Griewank and Notz (2013).

As the experiments from Notz et al. (2005) were conducted under pretty different conditions, I do not want to compare absolute values of bulk salinity. Moreover, I want to highlight that SAMSIM was tuned to simulate the not uniform desalination (varying bulk salinities from 7 ± 1 g/kg to 12 ± 1 g/kg in 2 cm to 14 cm ice depth) after 72 hours of freezing in the measurements of Notz et al. (2005) from both experiments. Forced by the lab measurements of temperature, SAMSIM can also simulate a very uniform salinity in the ice column which can be seen for 16-cm-thick ice from 2 cm to 12 cm depth in my experiments (compare Figure 18 right and Figure 17, left).

Furthermore, the bulk salinity for both experiments of Notz et al. (2005) differ for equal ice depths of about 1 *pm* g/kg to 5 g/kg. Therefore, I would interpret the generally higher bulk salinity of SAMSIM, in comparison to my measurements, not as a physical misunderstanding of gravity drainage. Moreover the underestimation seems to raise from the spare number of measurements, collected under similar boundary conditions, available to fit the free parameters of gravity-drainage parameterization in SAMSIM.

8 How homogeneous is growing sea ice in thickness, temperature and salinity?

8.1 Several wireharps in one single tank

As **Exp_20_1** was proceeded with one wireharp, I could only observe the solid fraction and salinity evolution at one single spot in the ice. In the following, I want show the results of experiment **Exp_15_3_A** which was conducted with three wireharps located in one single tank. The question after differences and similarities between the measurements at different locations can be considered as a case study of homogeneity of sea ice in general. This is an urgent question, considering that ice-core measurements only cover a single sample of sea ice and a lot of vertical and horizontal information about salinity and solid fraction can be lost, as global earth system models often assume sea ice to be homogeneous.

The ice growth in the tank was observed with three wireharps at different locations as schematically shown in Figure 6, the numbering of location and wireharp is equal in this context. The cooling temperature in the chamber was set to -15 °C and the heating wires were supplied with a power of 200 Watt. The measured parameters during the experiment were the same as for **Exp_20_1**, explained in section 6. Furthermore, the ice growth was simulated with SAMSIM individually for all three locations, forced by the respecting T_{top}.

8.2 Ice thickness evolution at different locations

The locations of wireharp 1, 2 and 3 were chronologically chosen from the left to the right side of the tank. The ice did not grow simultaneously fast at the 3 locations in the tank, see Figure 19. It took about 7 days until the ice grew to 16 cm at location 3, 8.5 days at location 2 and almost 9 days location 1.

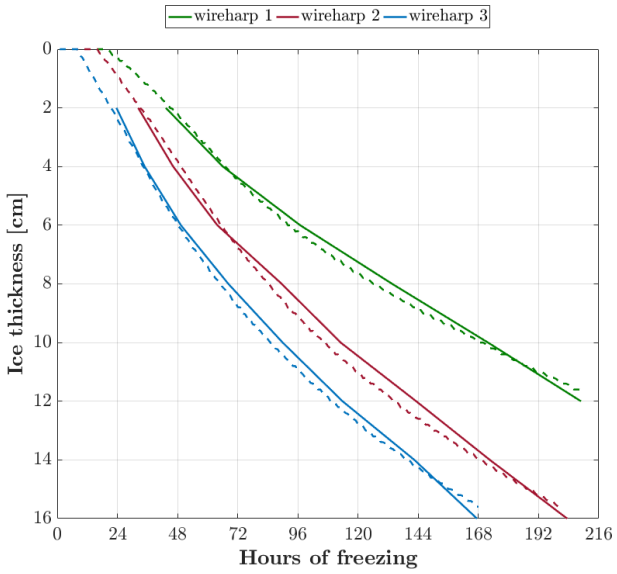

Figure 19. Temporal evolution of ice thickness for lab experiment **Exp_15_3_A** observed at three different locations in the tank (measured (solid line) and simulated (dashed line) ice thickness.

As the ice grew the fastest at location 3, which was furthest away from the cooling system, I suspect two different reasons for the irregular ice growth: The air is not as well-ventilated above the ice as it would be needed to create a homogeneous heat flux at the ice surface for all 3 locations. Additionally the convection of the water beneath the ice could cause different heat fluxes from the underlying water.

Concerning the agreement between measured and simulated thickness, the temporal difference in ice thickness is smaller equal 5 hours and also the start of ice growth is well-simulated for all three wireharps. The chosen heat fluxes for wireharp 1, 2 and 3 were set to 65 Watt, 58 Watt and 60 Watt and were chosen in agreement with the measured ice thickness. I would expect the difference in ice thickness be caused by the air temperature because the heat fluxes of the water in the simulation are more or less equal.

8.3 Surface-temperature deviation

For each wireharp, there was an individual simulation setup forced by the top temperatures calculated from the respective temperature profiles. For all three simulations, the simulated temperature profiles agree very well with the measured profiles, shown in Figure 20 and Figure 21. Only for location 2 and 3, the measured temperature in 2 cm depth differs more (from about 0.2 °C to 0.5 °C) than in greater depths from the simulated profiles . This small offset can be explained by the differ-

ence in the simulated and measured ice thickness. SAMSIM is forced by the ice-top temperatures at a certain time and the temporal difference of ice thickness in lab measurements and simulation leads to an offset between the temperature profiles which can be seen the strongest in 2 cm ice depth.

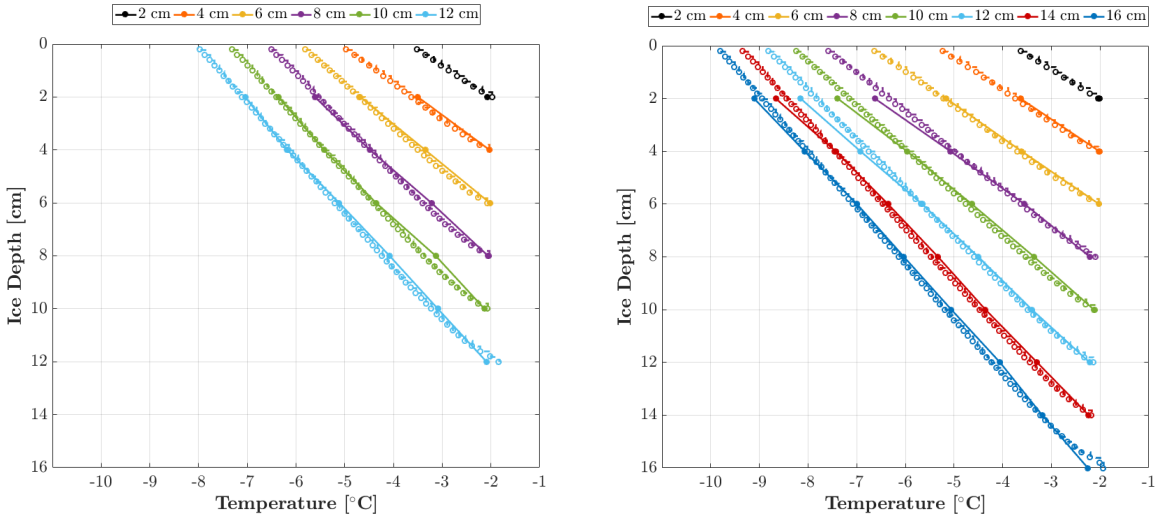

Figure 20. Measured (solid dots and line) and simulated (blank circles and dashed line) temperature profiles for increasing ice thicknesses (colors) of Location/wireharp 1 (left) and 2 (right).

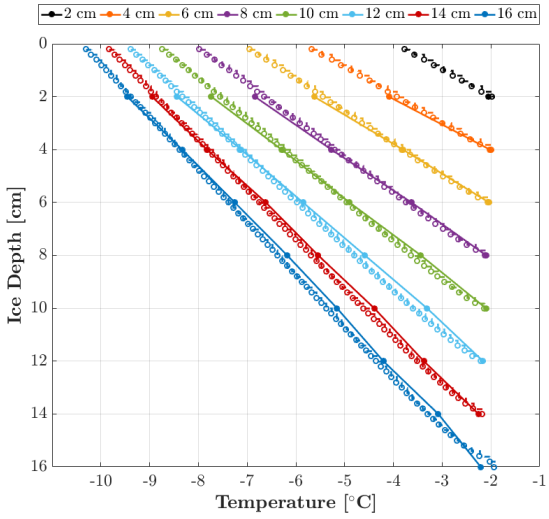

Figure 21. Measured (solid dots and line) and simulated (blank circles and dashed line) temperature profiles for increasing ice thicknesses (colors) of Location/wireharp 3.

Time [h]	wire harp	h_{ice} [cm]	T_{top} [°C]	$\triangle$T [°C]
	1	2	-3.5	
48	2	4	-5.2	≈ 3.5
	3	6	-7	
	1	8	-6.5	
144	2	12	-8.8	≈ 3.3
	3	14	-9.8	
	1	10	-7.3	
168	2	14	-9.3	≈ 3
	3	16	-10.3	

Table 4. . List of ice thickness (h_{ice}), surface temperature (T_{top}) at the three locations for a certain time of freezing (Time). The gradient in T_{top} (ΔT) between the coldest (3) and the warmest location (1) was calculated.

From the temporal thickness evolution, shown in Figure 19, I could see that for certain times, temperature profiles of different ice thicknesses can be compared among the three wireharps. Though I have chosen 48, 144 and 168 hours and the respective measured/simulated ice thicknesses h_{ice} of the wireharps. The chosen thickness profiles are listed in Table 4: T_{top} is the simulated surface temperature of the respecting thickness profile. T_{top} is simulated but I assume these temperatures to represent very similar top temperatures in the tank. From T_{top}, I derived the total horizontal temperature gradient between the warmest and the coldest location (1 and 3) $\triangle$T. As $\triangle$T is about 3 °C, it seems that temperature profile within the ice in the tank is very sensitive to air conditions and that the growing sea ice is heterogeneous in temperature across the tank.

8.4 Solid fraction and bulk salinity at different locations

The simulated and measured profiles of solid fraction and bulk salinity at the three locations are shown in Figure 22, Figure 23 and Figure 24. For all three simulations, SAMSIM generates almost the same absolute values and shape of bulk salinity and solid fraction profiles for increasing ice thicknesses. The simulated profiles also coincides with the simulated profiles of **Exp_20_1**. There is a very high simulated salinity at the ice surface (about 25 g/kg), a low salinity in the interior (about 10 g/kg), and increasing values from about 4 cm above the ice bottom, towards the bottom. In contrast to the similar simulated profiles, the measured profiles are more or less different from each other. I will briefly explain them separately.

Wireharp/Location 1: The sea ice at location 1 grew the slowest comparing to location 2 and 3. The highest solid fraction can be found in 2 cm depth and becomes more and more uniform for increasing ice thicknesses, except at the ice bottom. Reaching an ice thickness of about 12 cm, the measured salinity is about 4.8 to 5 $\pm$ 1 g/kg in the upper layers. The simulated profile shows a bulk salinity of about 10 g/kg (except the first 2 cm) in the upper layers. The measured solid fraction is slightly higher than the simulated values, the thicker the ice becomes. The solid fraction increases up to 0.95 in 2 cm depth for 16-cm-thick ice. In the upper layers, the solid fraction is pretty uniform and shows a decrease towards the ice bottom.

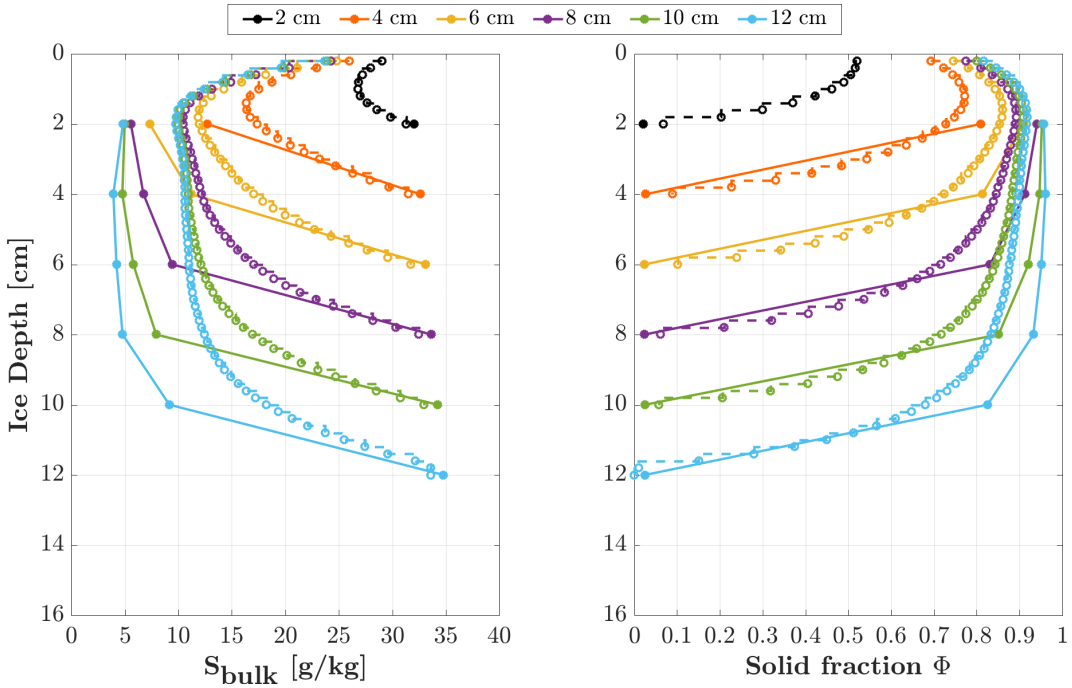

Figure 22. Location/ Wireharp 1: Bulk salinity and solid fraction profiles for increasing ice thicknesses (colors), Measurements (solid dots and lines) and simulation (blank circles and dashed lines) from wireharp 1.

Wireharp/Location 2: The measured desalination at location 2 seems to be as strong as at location 1 (see Figure 22). The absolute values of bulk salinity in the upper ice depths sink to about 4.6 to 5 ± 1 g/kg within even if the ice grew 4 cm more than at location 1. The bulk salinity is not uniform in all upper layers as it was seen for location 1. However, the measured solid fraction is also about 0.95 from 2 cm down to 10 cm depth, for the thickest ice. Comparing the measured profiles with the simulations, the findings of location 2 coincide with location 1: SAMSIM overestimates the bulk salinity by about 5 g/kg and underestimates the solid fraction by 0.05.

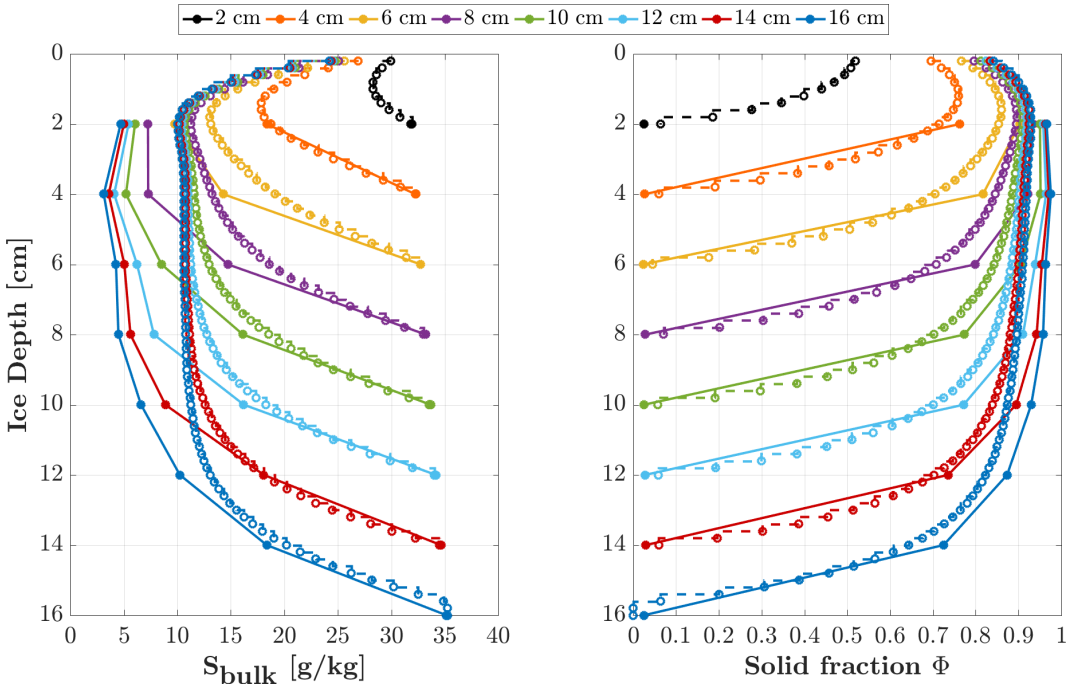

Figure 23. Location/Wireharp 2: Bulk salinity and solid fraction profiles for increasing ice thicknesses (colors), Measurements (solid dots and lines) and simulation (blank circles and dashed lines) from wireharp 2.

Wireharp/Location 3: Generally, the bulk salinity is higher for all ice thicknesses at location 3 than at location 1 and 2. The shape is also a bit different: The profiles do not show an uniform bulk salinity in the upper layers. The bulk salinity in 2 cm depth sinks to about 6.5 ± 1 g/kg during the ice grew 16 cm. For greater ice depths of all profiles, there can be seen a slight decrease of about 5 ± 1 g/kg until the bulk salinity increases fast towards the bottom. In general, it seems that the ice desalinated less strong at location 3 in comparison to location 1 and 2. Even if SAMSIM simulate a slightly different shape of the measured profiles, the absolute values of bulk salinity do agree slightly better with the measurements than for location 1 and 2.

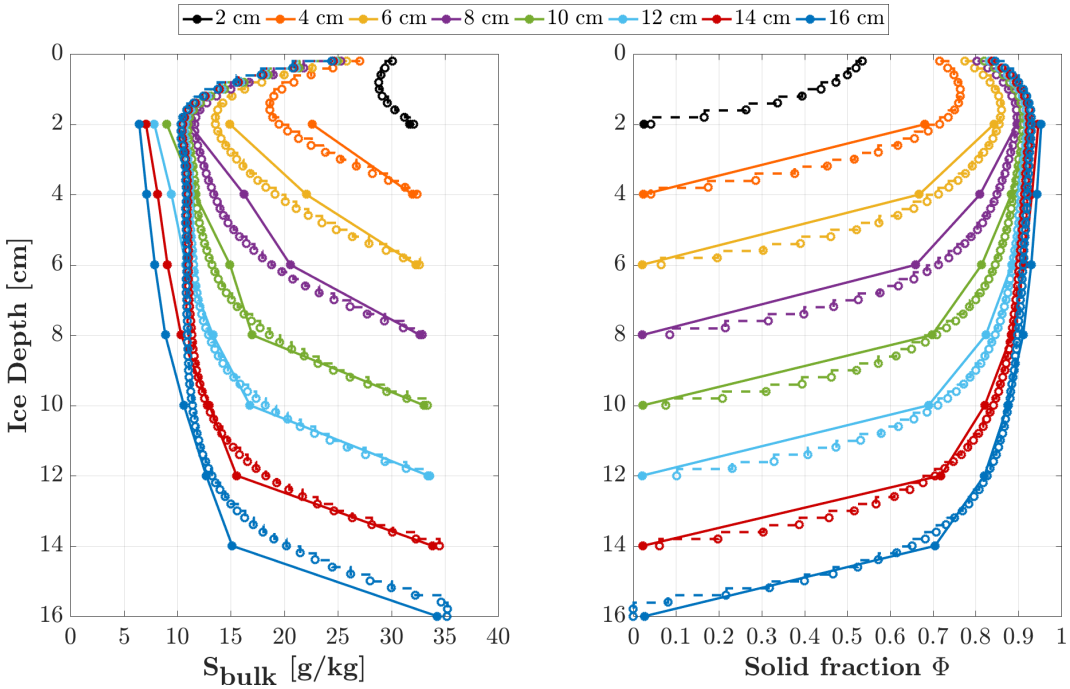

Figure 24. Location/Wireharp 3: Bulk salinity and solid fraction profiles for increasing ice thicknesses (colors), Measurements (solid dots and lines) and simulation (blank circles and dashed lines) from wireharp 3.

8.5 Sensitivity to ice temperatures

In general it can be said that the ice in the tank was inhomogeneous in thickness, temperature, solid fraction and bulk salinity at the three different locations. The main reason for that was found to be the gradient in air temperature across the tank and the resulting different ice-surface temperatures at the three locations. The total simulated surface temperature gradient across the three locations was about 3 °C to 3.5 °C. Location 1, in the left part of the tank (half-shielded part) was the warmest and location 3, the coldest. The surface temperature of the central location 2, was approximately between the surface temperature at location 1 and 3.

The most obvious conclusion of the comparison between the measured profiles at the three locations in thank is that the ice grew the fastest at the coldest location and the slowest at the warmest location. The measured bulk salinity at the coldest location is up to 5 ± 1 g/kg higher for the upper layers than for location 1 and 3. SAMSIM simulates ice thickness and temperature very well (highest absolute deviation is 5 hours for thickness and about 0.3 °C for temperature) but the calculated solid fraction and bulk salinity profiles are almost the same for all three locations.

The best agreement in absolute bulk salinity and solid fraction can be seen for the third location. On the other hand, the shape of simulated solid fraction and salinity profiles agree better with location 1 and 3 because both show a uniform bulk salinity in the interior of the ice. For location 3, the bulk salinity increases slowly by 5 $\pm$ 1 g/kg from the top towards 4 cm above the bottom. Even if there is a surface temperature gradient between location 1 and 3, the absolute salinity in the interior and the shape of the profiles are more similar than comparing location 2 and 3.

The measured absolute values of bulk salinity differ at the three locations but the simulated profiles of SAMSIM remain the same even if they were forced by the individual temperature profiles. Besides, SAMSIM overestimates the bulk salinity in the interior and underestimates the solid fraction. It simulates the shape of bulk salinity at location one and three well. As a uniform bulk salinity could not be found at location three, the shape of measured and simulated profiles differ the most. In absolute values, the simulated salinity and solid fraction agrees better with the measured profiles at location three, as the measured bulk salinity at location three is higher than at location one and three. This coincides with lab experiments by Cox and Weeks (1975) and Wettlaufer et al. (1997) who measured that more salt is retained in growing sea ice, the colder the cooling temperature. In model studies by Griewank and Notz (2013) it was found that both, solid fraction and brine salinity, are slightly higher for lower freezing temperatures. In relation to the Rayleigh number, Equation 9, I would explain that lower freezing temperatures lower the permeability due to initial higher solid fractions. A lower permeability coincides with a lower Rayleigh number and results in an later onset and less strong gravity drainage. I would not consider the irregularity in the brine channel system as the reason for the heterogeneity in bulk salinity across the locations. The heterogeneity in brine channels, was found by (Cottier et al., 1999) to only occur on horizontal scales of 10 cm. The wireharps had a greater distance between each other.

From the comparison of solid fraction and bulk salinity across the three locations, I would conclude that the gravity drainage of SAMSIM is not as sensitive to freezing temperatures as it would be required. On the other hand, this is just one exemplary experiment at three locations and the observation of heat fluxes (water and air) was limited. An increase in the reliability of measurements could probably be caused by the repetition of the experiment under very similar boundary conditions. This was aspired by repeating the experiment **Exp_15_3_A** under the same boundary conditions, called **Exp_15_3_B**. Unfortunately one of the two pumps fell of the wall

of the tank during **Exp_15_3_B** what caused an insufficient mixing of the water in the tank. As a consequence, the ice grew much slower and even more heterogeneous within the tank as it was the case for **Exp_15_3_A**. I decided that a comparison between these both experiments would not be gainful for improving SAMSIM's parameterization of gravity drainage.

9 Period of stabilization

After the ice had grown to 16 cm, the melting was not directly introduced. There is an interim time between freezing and melting, I will call this time, period of stabilization in the following. It was introduced when the last wire pair was enclosed with ice. The air temperature of the cooling chamber was then set to -10 °C to generate a smaller temperature and brine gradient within the ice. Unfortunately, there is a lack in the measurements of temperature and resistance during this time for **Exp_20_1**. But from the whole time of recording (see Figure 35, left) it can be seen that when the temperature in the cooling chamber increased (after about 150 hours of recording), the resistance measurements of the upper ice layers (2 cm to 10 cm depth) dropped to a certain resistance value. This resistance is very similar to the value which was measured when the recording of data started again (after about 210 hours). From other experiments which were proceeded the same (Freezing, Stabilization and Melting) it can be seen, that the resistance and temperature stay nearly constant, after dropping due to warmer air temperatures and before melting was introduced.

This period of stabilization was simulated the same way as the freezing process with SAMSIM. T_{top} was derived by the temperature gradient within the ice and SAMSIM was forced by its temporally interpolated evolution. The temperature, salinity and solid fraction profiles, simulated by SAMSIM and the profiles of the lab measurements after the period of stabilization are shown in Figure 25 and Figure 26.

The measured profiles of solid fraction and bulk salinity changed slightly after the period of stabilization. The simulated profiles do not show any further desalination, either the ice grew about 2 cm in the simulation. The temperature gradient is smaller within the ice, but still consistent, low temperatures, due to the cold air, are measured at the top and are linearly increasing over the whole ice depth.

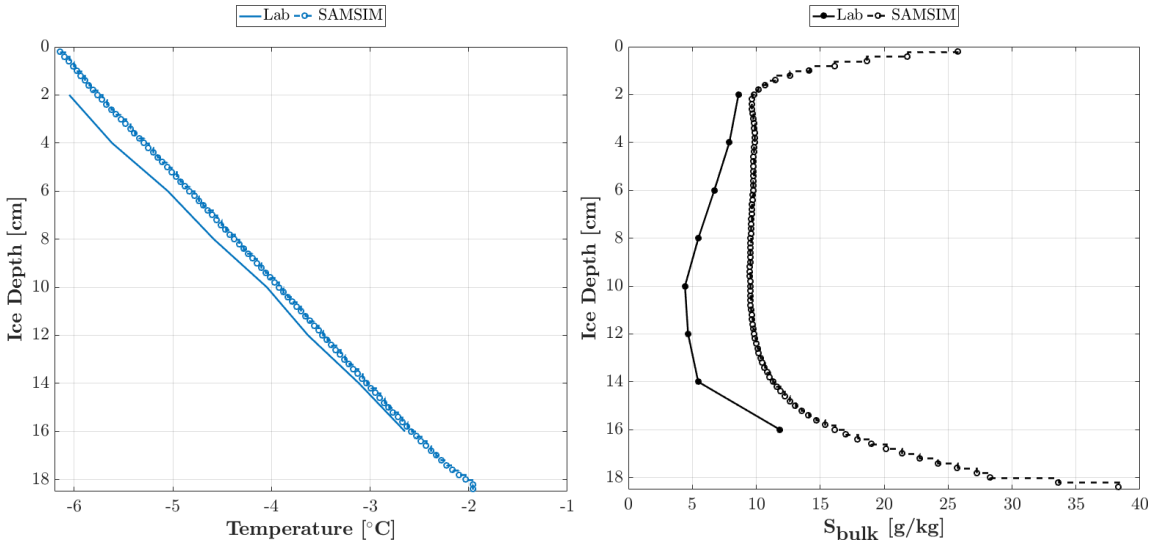

Figure 25. Measured (solid dots and line) and simulated (blank circles and dashed line) temperature (left) and bulk salinity (right) profile after the period of stabilization.

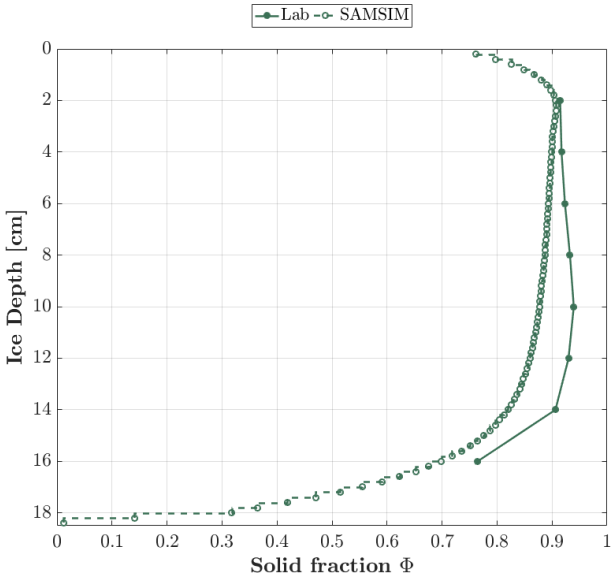

Figure 26. Measured (solid dots and line) and simulated (blank circles and dashed line) solid fraction after the period of simulation.

The profiles of solid fraction and bulk salinity changed a bit during the period of stabilization: It seems that gravity drainage has further decreased the salinity in ice depths from 4 cm to 14 cm depth, so that the profile has been 'buckled' towards a lower salinity in these depths. The salinity in the upper most 4 even increased slightly (compare therefore Figure 25 with Figure 17).

The reason for that might be, that the cold temperatures at the top and the high solid fraction decrease permeability as far as gravity drainage cannot occur because

a critical Rayleigh number could not be reached any more. In the downer layers, the bulk salinity was already pretty low but the temperatures are higher than in upper layers which coincide with a higher permeability. This could cause a critical Rayleigh number in the dower layers and further desalinated the ice.

10 Which processes of desalination does the wireharp observe during melting?

10.1 Boundary conditions during melting

The melting of sea ice was introduced by setting the air temperature in the cooling chamber to +5 °C. The air over the ice became stable layered, because the ice is cooling the air from underneath. The measured air temperature in 10 cm height above the ice was therefore about -3.8 ± 0.01 to -1.5 ± 0.01 °C (shown in Figure 27, left).

The melting experiment is treated as a single experiment and not in attachment to the freezing and stabilization process. This is why the temporal evolution of measurements in this chapter are starting with zero hours, even if the recording of data started with the freezing process.

The CTD measurements show that the water temperature increased slightly and water salinity decreased during melting (see Figure 27, right). The water salinity had increased to about 40 ± 0.001 g/kg during the process of freezing and stabilization. After setting the air temperature in the room to 5 °C, it took about 115 hours to reach a stable water salinity of about 33.3 g/kg, which is about 0.2 g/kg higher than the salinity measured in the beginning of the experiment. The risen salinity is very likely due to evaporation during the experiment.

The melting can be seen in the water temperature as a slow increase until about 110 hours after melting has started (see Figure 27, left). Afterwards, the water temperature increases linearly stronger what indicates that the water was warmed by the air and no ice was consuming energy for melting anymore. A stable water salinity was reached after about 110 hours, what I would identify as the time of completely melted ice in the tank. This is a crucial information because the wireharp can only measure ice thicknesses which have shrinked to 2 cm. The ice got very porous, permeable and irregular in thickness across the tank during melting (see a snap shot of the tank in the end of melting in Figure 28). Therefore it is not trivial to identify the current ice thickness within the resistance measurements

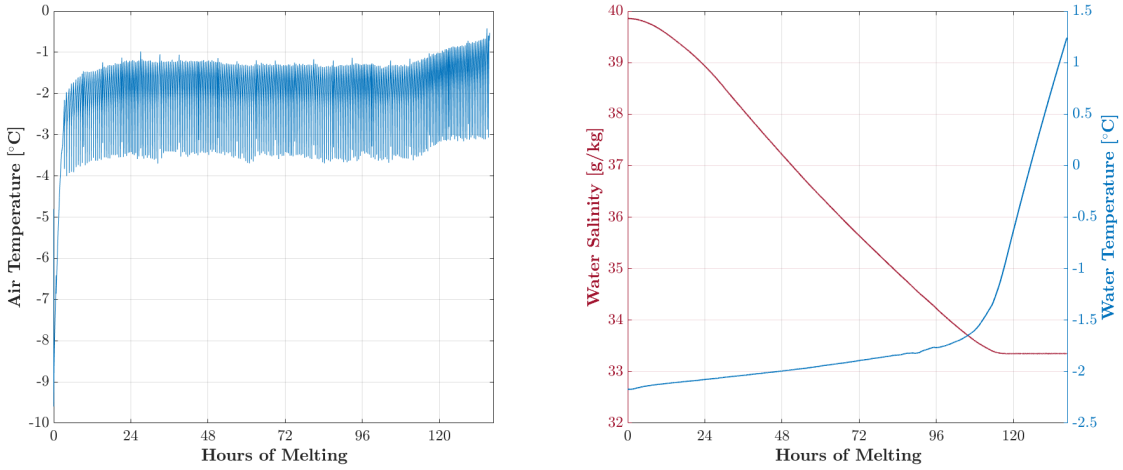

Figure 27. Left: Water temperature and salinity evolution during melting, measured by the CTD in the middle of the tank. Right: Air temperature in 10 cm height above the ice where the wireharp was installed.

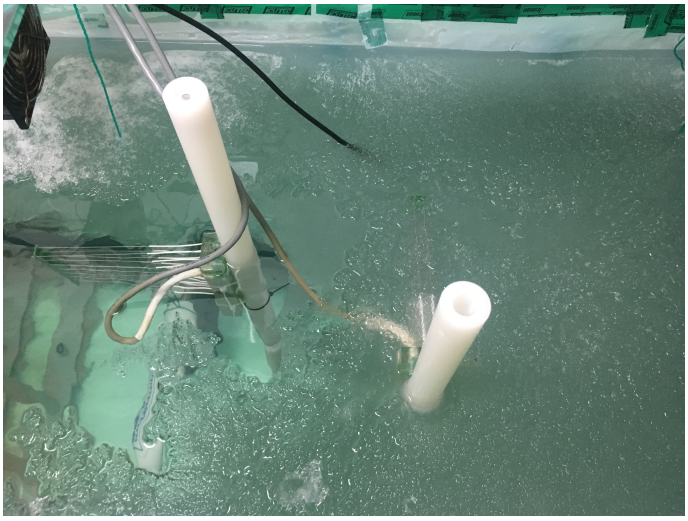

Figure 28. Picture of a melting experiment with several wirharps. One wireharp is already totally ice-free while another one is still frozen.

10.2 Stages of melting

Up to now, there do not exist continuous in-situ measurements of solid fraction and salinity in melting thin sea ice. Therefore I will present the measurements of the wireharp and interpret the data in the way that I link the results to physical processes which might be occured.

As it could be seen in Figure 25 and Figure 26, the absolute values of solid fraction, temperature and bulk salinity changed during the period of stabilization. Addition-

ally, in the beginning of melting, the highest resistance is not measured in 2 cm depth any more as it was the case for freezing. Rather the highest resistance can be found in 10 cm depth followed by the resistance in ice depths of 8 cm, 12 cm and 6 cm (see Figure 29, left). However, the calculated solid fraction in all depths, except in 16 cm, is very similar of about 0.92. The temperature gradient within the ice became less strong during the period of stabilization and the bulk salinity is the lowest in the interior of the ice (see Figure 30. In the following, I have divided the melting measurements in three stages, titled as I: initial warming, II: Increase in solid fraction and bottom melt, and III: melting in all depths. The temporal evolution of resistance, solid fraction, temperature and bulk salinity in the respective ice depths are shown in Figure 29 and Figure 30. I will discuss these stages of melting separately because of different observed physical processes.

I: Initial warming

After the air temperature was switched to +5 °C, the ice temperature becomes almost homogeneous within about 18 hours (see Figure 30, left) and also the resistance measurements decrease for all ice depths as the ice becomes warmer. The resistance in 14 and 16 cm ice depth shows a slightly stronger decrease than in the upper layers. They are warmed by the heat flux from the water. At the end of period I, the solid fraction in 14 cm and 16 cm decreases to 0.65 and 0.75, while the upper layers just decrease to a solid fraction of about 0.9. An exception is the wire pair in 2 cm depth. Its resistance sinks nearly as strong as the resistance over the wire pair in 14 cm depth. The upper most wire pair feels the warmer air over the ice the most because the air temperature directly above at ice surface is between -1.5 ± 0.1 °C and -3.8 ± 0.1 °C. During this time, the salinity increases in 14 cm and 16 cm depth due to a decreasing solid fraction and increasing temperatures while the salinity from 4 cm to 12 cm depth stays constant and the salinity in the upper most 4 cm sinks slightly from 8 ± 3.3 g/kg to 6 ± 3.3 g/kg. The large error in bulk salinity will be explained in the third stage of melting.

The fact that the 2 upper most wire pairs measure a lower solid fraction in this first period of melting, I would identify as melting at the ice-air interface. Additionally, the ice starts to melt at the bottom what can be seen as the strong decrease in solid fraction after about 12 hours in 14 cm and 16 cm depth. The ice experiences almost no melting in 12 cm, 10 cm, 8 cm depth at this time, as the solid fraction stays constant. This can be seen in the temperature measurements after about 10

hours when the ice in the upper 4 cm becomes warmer than the ice in 12 cm, 10 cm and 8 cm depth due to the warming of fresher melt water. The bulk salinity stays almost constant in all depths, just a slight decrease can be seen in 2 cm and 4 cm depth.

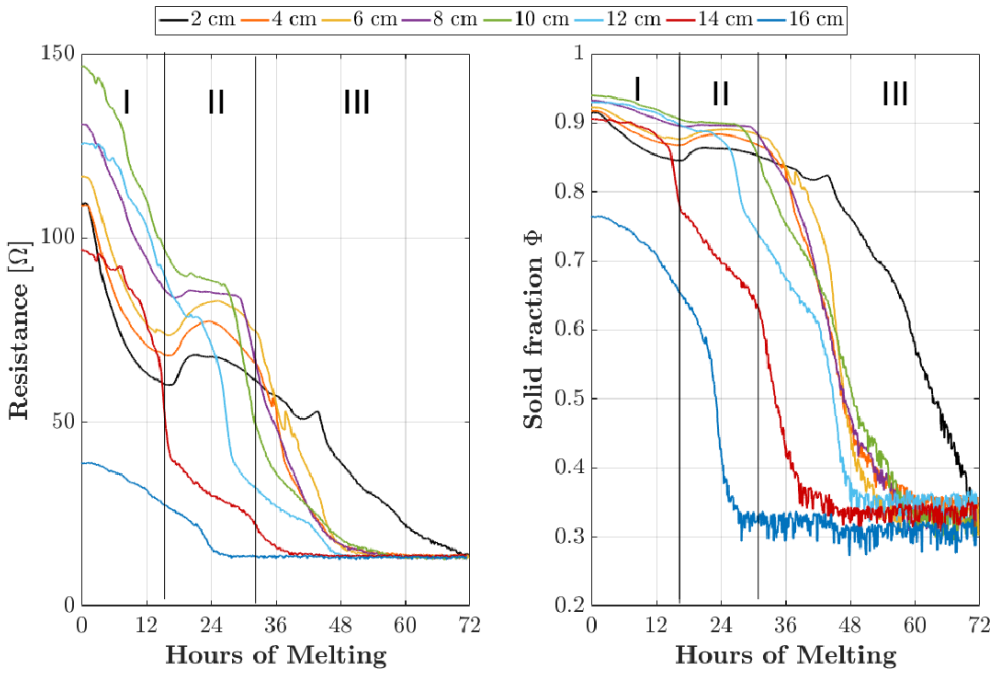

Figure 29. Stages of melting I, II and III. Temporal evolution in ice depths (colors) of resistance (left) and solid fraction Φ (right) during melting.

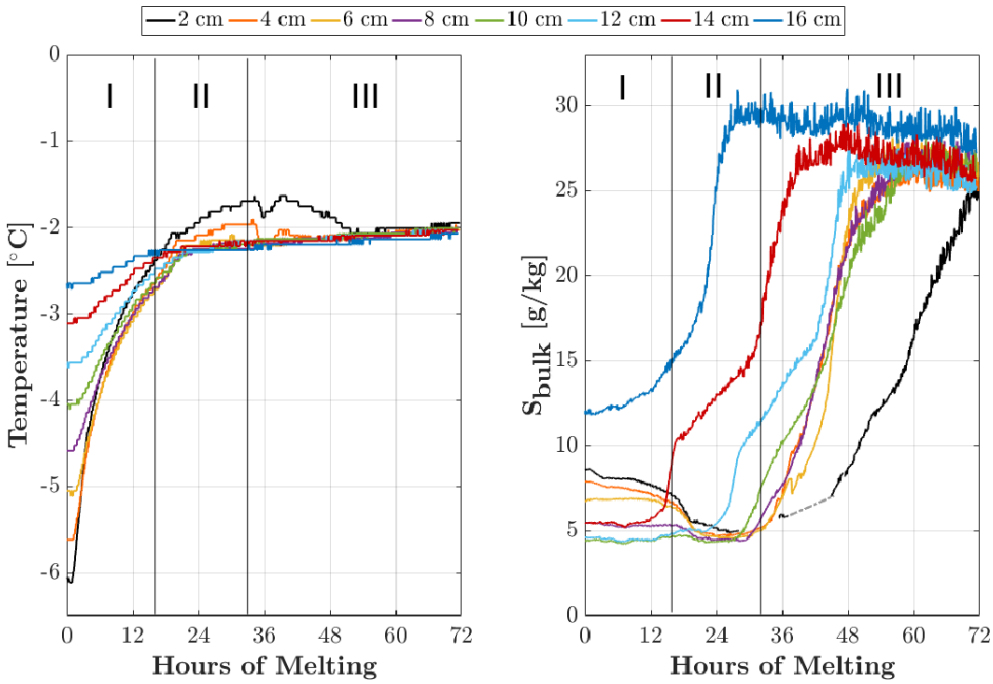

Figure 30. Stages of melting I, II and III. Temporal evolution in ice depths (colors) of temperature (left) and bulk salinity (right) during melting.

II: Increase in solid fraction and bottom melt

After 18 hours of melting, the general decrease resistance and solid fraction changes. In between 18 and 32 hours of melting, the resistance and solid fraction increases slightly again in 2 cm to 6 cm depth whereas the resistance in 8 cm, 10 cm and 12 cm depth stays constant. The resistance in 14 cm and 16 cm sinks to a resistance which is slightly higher than the resistance of pure water which was measured before ice growth. This indicates that there is an error in the resistance measurements. This may be caused by the circumstance that the data cable of the wireharp was removed from the circuit board during the period of stabilization. This is additionally the reason why the data of the time between freezing and melting is not recorded for **Exp_20_1**. The plug of the wire-harp cable at a later time may be disturbed by frozen water or salt crystals, which could cause the measured offset in resistance. However the reason for the offset can not be explained properly. It can just be said that this behavior was not found for the other experiments when no removal of the curcuit board took place.

The error in bulk salinity due to the uncertainty of R_0, the resistance of pure water was calculated for the offset in resistance of about 5 Ω which was recorded in the end of the experiment. For a solid fractions above 0.8 it was found that the offset in R cause an increase of ΔS_{bulk} up to 3.3 g/kg and increases further for solid fractions smaller than 0.8, up to 15 g/kg (see also Figure 37). Therefore, values of S_{bulk} for solid fractions smaller than 0.8 cannot be treated as absolute for this melting experiment, rather the temporal evolution was considered to explain the processes.

Simultaneously to the increase in solid fraction, the temperature increases up to -1.5 ± 0.1 °C in 2 cm depth and up to -2 ± 0.1 °C in 4 cm depth. The deeper sensors measure a temperature of about -2.3 ± 0.1 °C. The exceed of freezing temperature in the upper 4 cm might be caused by ice and melt water which can be warmed to this temperature because of its low salinity content. The resistance measurements show an increase for the upper 6 cm and the resistance in 8 cm and 10 cm depth stops decreasing. This coincides with an decrease and stagnation in solid fraction.

The increase in solid fraction must be caused by water that refreezes. That can be introduced by flushing, so water with a low salinity content which travels downwards through the ice, and mixes with/ drains out the liquid brine in deeper ice layers. When the brine is diluted by melt water, it can freeze again until the amount of

brine is reached what coincides with the ice temperature (respectively Equation 2) and its solid fraction increases. This process would decrease the salinity content as it can be seen in 2 cm, 4 cm and 6 cm depth if the melt water mixes the brine and travels further through the ice. So brine with a lower salinity content would remain in the pockets and lower the bulk salinity in the respective ice depth.

The solid fraction in 12 cm and 14 cm depth sinks continuously after a certain time (about 14 hours) and the ice has already been melted completely in 16 cm depth. The values of solid fraction cannot be treated quantitatively after falling below 0.6 because of the offset in resistance measurements. Therefore a solid fraction of 0.3 is caused by the offset in R_0 and must be interpreted as a solid fraction of 0, pure water.

III: Melting in all depths

During the third stage of melting, there are just 14 cm of ice left and the solid fraction decreases fastly in all depths and reaches a solid fraction of 0.3 (respectively 0, pure water) at a certain time (see Figure 29, right), from about 40 hours to 68 hours what makes it nontrivial to say how thickness evolves during this time. I suspect that the melting ice bottom becomes very rugged due to the strong circulation in the tank and the high heat input by the heating wires. This could be an explanation for the circumstance that the wire pairs in 10 cm to 4 cm measure a resistance drop to the resistance of pure water shortly.

The bulk salinity increases as fast as the solid fraction decreases (see Figure 30, right). Specially, the salinity increases for all ice depths even if ice beyond a certain depth has not melted totally. That thinner ice than 12 cm, melts simultaneously as the solid fraction decreases and the bulk salinity increases at the same time. That indicates that melt water in the interior of the ice must be replaced by underlying water, otherwise the salinity would stay the same in an ice depth before the layer below has melted completely.

The temperature gradient across the ice thickness is almost zero during the third stage (see Figure 30, left). The temperature in 2 cm depth, which has increased to about -1.5 $\pm$ 0.1 °C in stage two, sinks slightly, increases again for several hours and decreases finally to the freezing temperature of water. This behavior in temperature, which also can be found in 4 cm, but for slightly lower temperatures, coincides with an short increase in solid fraction in 4 and 2 cm depth after 37 and 42 hours.

Probably these ice depths experience a melting effect in stage three, resulting in a lower solid fraction and melt water which can warm to a higher temperature. After a certain time, about 72 hours, the temperature in all depths increases homogeneously to the freezing temperature and the bulk salinity increases for the upper layers.

11 Is it possible to simulate the melting process with SAMSIM?

As it was mentioned before, there do not exist continuous measurements of temperature, solid fraction and salinity in melting sea ice. I therefore investigate if SAMSIM is able to simulate the measured profiles during melting. The flushing parameterization in SAMSIM is based on different assumptions, discussed later on, which were found to be able simulating the salinity profile of ice cores, taken during the melting season (Griewank and Notz, 2015). Up to now, there do not exist model studies how far this parameterization is able to reproduce the salinity evolution in thin sea ice. This chapter explains and discuss the attempt to simulate the melting of **Exp_20_1** with SAMSIM. I will first show the results of a comparison between measured and simulated profiles of temperature, solid fraction and bulk salinity profiles and discuss how it reflects the assumptions of SAMSIM concerning flushing.

The forcing of SAMSIM during melting differs from simulating the freezing process. The freezing was simulated by deriving the top temperature of the water/ice, time-depended. This method was found to be not suitable to simulate the melting in SAMSIM. I have chosen the way of initializing profiles of specific enthalpy, total mass and the absolute salinity of the different layers in SAMSIM. These profiles originate from the end of the total simulation of freezing and period of stabilization. As the model was fed by profiles of already existing ice, the melting was introduced by a respective positive heat flux from the air or/and the water. The heat exchange between ice and air in SAMSIM is derived by the assumption that the heat flux is proportional to the gradient between the top-layer temperature and the air temperature in 2 m above the ice. So the melting was forced by setting the air temperature in the model setup to +5 °C and the heat flux from the water to 50 Watt.

11.1 Simulated and measured ice thickness and temperature evolution

Concerning the measured ice thicknesses/depths of the profiles shown in Figure 31 and Figure 32, it must be mentioned that they do not contain surface ablation as no surface ablation about 2 cm was measured in the tank. The ice depth on the y-axis is the respective depth where the wire pairs and temperature sensors were frozen

during the freezing process. Additionally it is not trivial to define the ice depth to a certain time as already could be seen in the resistance measurements. Therefore I have chosen the time of profiles whenever the resistance over a wire pair reaches the resistance of pure water. This is not the resistance R_0 as it was measured before freezing for **Exp_20_1**, as already explained. Therefore I have chosen the thicknes profiles whenever a wire pair showed a stable resistance. The times of measured ice thickness can be seen in comparison to the simulated thickness in Figure 31 on the left.

The bottom heat flux was assumed as 50 Watt what is 10 Watt higher than the heat flux which was chosen for the freezing and the stabilization period. The reason for that was the slightly better matching thickness evolution of measurements and simulation. It could be explained that the heat flux from the heating wires is more warming the water as the ice shrinks at the sides during melting and the water can be warmed by the air at the sides. As another reason for a complicated identification of ice thickness, I would suppose that the ice becomes very rough at its bottom. Additionally, the convection which is generated by the pumps in the tank, could be responsible for a not very homogeneous ice thickness retreat during melting.

As it could be seen in Figure 30 the temperature gradient which existed through the period of stabilization disappears within 16 hours after introducing melting. The temperature decreases to about -2 °C in all ice depths, that can be seen in the thickness profile of 16 cm, see solid lines in Figure 31, right. The ice temperature in the upper most 6 cm is even slightly higher than the water at the ice-water interface. I would explain these temperature profile by a relatively high solid fraction, so not much ice has melted away until this time but a low bulk salinity in the upper 6 cm. For a decreasing ice thickness, the profiles of temperature stay at the freezing temperature.
The simulated temperature profiles differ a lot from the measured profiles. At the top of the ice, the temperature is about 0 °C and the ice shrinks, the deeper layers also become 0 °C. For an ice thickness of 16 cm the temperature sinks down to -2 °C from 10 cm to 14 cm depth and increases from 14 cm to 16 cm depth up to -1.5 °C. For the profiles of less or equal 14-cm thick ice, this behavior remains: the temperature in the upper layer/layers is about 0 °C, sinks to a certain value in a certain depth and shows a warming in the most lowest 2 centimeters.

These temperature profiles are caused by the assumptions of SAMSIM's complex

flushing parameterization approach. SAMSIM assumes a temperature of 0 °C for 0 g/kg salt during melting. The temperature of 0 °C at the top of ice, for all ice thicknesses, is caused by a complete desalination of the upper layers, due to simulated melt water at the top which is assumed to move vertically through the layers and washing out brine. Additionally, melt water can occur vertical and horizontal. Brine which is transported horizontally in SAMSIM, is assumed to reach a fictional 'crack' in the ice (as SAMSIM is only 1-D) and is flowing directly in the underlying water. So the most upper layer cannot become fullfully liquid because the layer is then assumed to be completely melted and the melt water is removed. SAMSIM assumes this melt water as been flown through a crack and transported into the lowest most layer of the model. The temperature increase at the bottom of the ice is due to the positive heat flux. The heat flux can warm the bottom layers strongly as the melt water in the lower layers is relatively fresh and can warm stronger than ice or salty water.

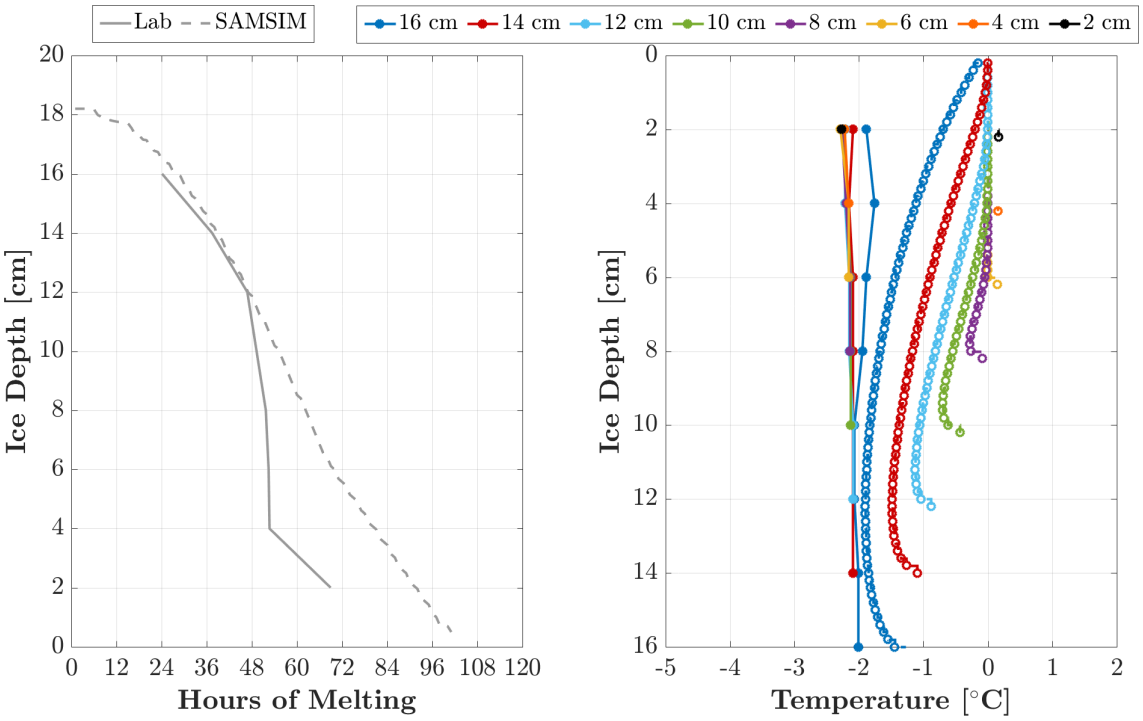

Figure 31. Measured (solid circles and line) and simulated (blank dots and dashed lined) temporal thickness evolution (left) and temperature profiles (right) for decreasing ice thicknesses (colors) during melting.

11.2 Measured profiles of liquid fraction and bulk salinity during melting

The behavior of measured liquid-fraction and bulk-salinity profiles for decreasing ice thicknesses reflects the analysis of melting data, shown in Figure 29 and Figure 30. Until now, I compared measured and simulated solid fraction Φ, but for the melting process I will show the comparison of measured and simulated liquid fraction, what is simply 1- Φ. I compare the profiles for decreasing thicknesses but it must be said that the ice thickness is a very unreliable parameter for the melting process, as the ice bottom becomes very rough and the complete melting of a layer is not trivial to identify in the resistance measurements.

For an ice thickness of 16 cm, the wireharp measured a liquid fraction which is low (about 0.1) in 2 cm depth, but relatively constant (about 0.3) for all ice depths from 4 cm to 14 cm depth. As the liquid fraction in an ice depth is 1, the ice is assumed to be fullfully melted. For an ice thickness of 14 cm, the measured profile of liquid fraction looks very different from the measured profile of 16 cm thick ice: The liquid fraction in 2 cm is still very low but increases much faster for greater ice depths, it increases from 2 cm to 12 cm depth, from 0.1 to about 0.6. The greatest ice depth of 14 cm depth is assumed as completely liquid. Until the ice has melted to 8 cm, the liquid-fraction profile is very similar to the profile of the 14-cm-thick ice. For a decreasing ice thickness, the liquid fraction becomes even higher in lower ice depths.

The evolution of the measured bulk-salinity profiles behaves very similar to the liquid fraction profiles, because of the non-existing temperature gradient within the ice. The liquid-fraction profile determines the bulk-salinity profile and leads to a slightly increasing salinity from the top to the bottom of about 5 to 10 $\pm$ 3.3 g/kg for an ice thickness of 16 cm. For an ice thickness of 14 cm, the bulk salinity stays about 5 $\pm$ 3.3 g/kg in 2 cm depth but increases linearly from 2 cm to 6 cm to 20 $\pm$ 3.3 g/kg and from 6 cm to 12 cm depth, it increases further to 25 $\pm$ 3.3 g/kg. The salinity of the lowest ice depth of every ice thickness is assumed as the salinity of the underlying water.

11.3 Simulated profiles of liquid fraction and bulk salinity during melting

The high difference between measured and simulated profiles of bulk salinity and liquid fraction raises from the complex flushing parameterization of SAMSIM. The simulated liquid-fraction profile of the 16-cm-thick ice shows a relatively high value of about 0.6 at the top and decreases fastly until it reaches about 0.35 in 2 cm depth. A relatively low liquid fraction is found between 2 cm and 12 cm depth and increases towards the bottom. The profile still has the C-shape, as it was simulated for the freezing process and for the period of stabilization, For an ice thickness of 14 cm, there can be found a liquid fraction on 0.2 at the top of the ice and for the profiles of decreasing ice thicknesses, this minimum increases with the ice depth. For decreasing ice thicknesses, there can be seen a small 'bump' of higher liquid fraction after the value was at constantly 0.2. After this small increase, it sinks again to about 0.2. The increase towards the ice bottom can be found in every profile and is mostly present in the lowest 4 cm of the ice.

The simulated bulk salinity profiles do not behave as similar to the liquid-fraction profiles as it was the case for the measurements. This raises from the simulated non-homogenoeus temperature profile, as it was measured. The bulk salinity in the upper most layers becomes 0 g/kg as deep as the liquid fraction is about 0.2 for the different profiles. In the beginning of melting, there is a smooth increase in bulk salinity from the top towards the bottom. It is followed by a strong increase due to the strong increase in liquid fraction in the lowest 4 cm of ice.

The increase in bulk salinity towards the bottom can be explained by brine which is flushed downwards from upper layers and increases their salinity by mixing with melt water. The bulk salinity at the ice bottom becomes lower for decreasing ice thicknesses. So for example, for ice what is about 16 cm thick, there can be found a relatively high bulk salinity of about 27 g/kg at the bottom and for an ice thickness of about 10 cm, there is a simulated bulk salinity of 15 g/kg. I suspect that there is fewer brine what can be flushed into greater depths for smaller ice thicknesses because the most of the brine has already been flushed before. This can be also seen in the simulated salinity, which becomes deeper and deeper 0 g/kg at the ice surface, for a decreasing ice thicknesses.

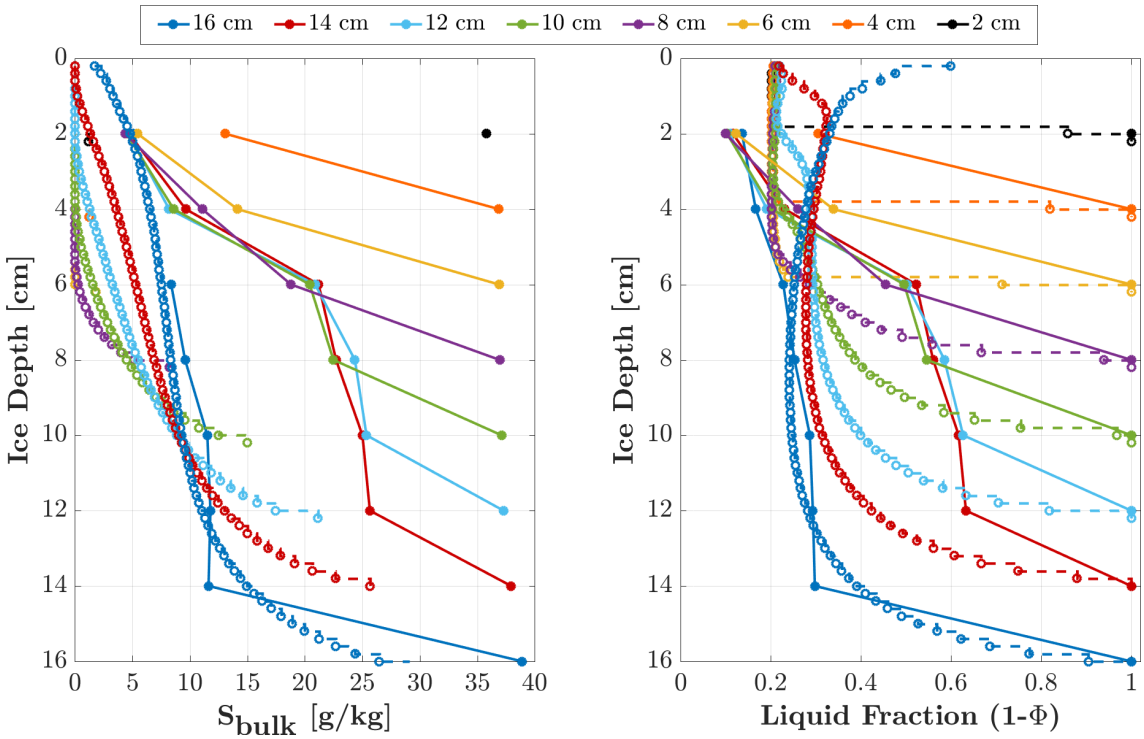

Figure 32. Simulated (blank circles and dashed line) and measured (solid circles and line) bulk-salinity and liquid fraction profiles for decreasing ice thicknesses (colors).

11.4 Flushing in SAMSIM

I will briefly sum up and discuss the important differences between measurements and simulation caused by the flushing approach in SAMSIM: The simulated surface temperatures result mainly from the salinity profile. A strong surface melting/ flushing, leads to a completely salt-free surface, what the simulated profiles show. SAMSIM assumes that the surface temperature is always 0 °C for 0 g/kg salt during melting. The increase in bottom temperatures is caused by the positive heat input from the water beneath. This high salinity at the bottom is caused by flushed brine, moving downwards to the ice-ocean interface, increasing the salinity of the bottom layers. Griewank and Notz (2015) already showed that their complex flushing parameterization leads do an increase of salinity close to the ice-ocean interface if gravity drainage is deactivated. The main difference between the measured and the simulated profiles of liquid fraction and bulk salinity is the increase of both from 6 cm depth towards the bottom (see Figure 32). The simulated profiles stay at a relatively low liquid fraction for the respective depths as well as the bulk salinity which is very low and even decreases for thinner ice. This can be explained as the simulated ice melts across the whole ice column. The melting desalinates the ice at the top by melt water which flows, due to the assumptions of the flushing

parameterization, vertically and washes out the brine in deeper layers. Horizontal flushing in all layers leads to melt water, being assumed to flow into a 'crack' and transporting heat and salt into the lowest layer of ice. Melt water due to surface melt is therefore not able to form melt ponds at the top of the ice, because SAMSIM removes the horizontal flushed water in all layers immediately when it is formed. The complete desalination of the upper layers could not be found in the measured data, where the salinity in 2 cm depth stays nearly constant at about 4 ± 3.3 g/kg and just a slightly lower salinity can be measured in 4 cm depth for a progressed melting process (comparing the salinity in 4 cm ice depth, 14 cm versus 12 cm ice thickness). As it was shown in subsection 10.2, a desalination of the upper layers only occured before the ice had melted to 16 cm.

The complex flushing approach was tested to simulate Arctic conditions (Griewank and Notz, 2015) and comparing salinity profiles with ice-core measurements which were taken at Barrow, Alaska during the melting season (Eicken et al., 2012). It was found that SAMSIM simulates the salinity profile of the ice cores very well with the complex flushing approach and the deviation did not exceed 2 g/kg, except the ice-bottom salinity. The ice cores showed a sharp increase in salinity at the ice-ocean interface but the simulated salinity even showed higher values. This is in contrast to my experiments which show much higher salinities for greater ice depths, due to convection. Futhermore the SAMSIM's flushing approach leads to a salt-free surface in summer, whereas the ice cores, taken in June and July show a salinity of about 1 g/kg at the top. In comparison to this, my experiments show a very small decrease of salinity in the upper layers for progressed melting. On the other hand the salinity of the upper layers is not known before melting, so it is not clear how much desalination occured due to flushing.

Furthermore, it is not trivial to estimate the heat flux in SAMSIM which is responsible for surface ablation. During the melting process, SAMSIM simulated a total surface melting of about 8 cm. In the lab experiments, the wires of the wireharp were still completely covered by water in the end of the experiment. As the wireharp was installed to move up and down, the surface melting could not exceed 2 cm for my experiment. The measured and simulated profiles of ice thicknesses which are compared in Figure 31 and Figure 32 are therefore not representing the same ice layers.

The wireharp stayed solid in one ice depth after freezing and the ice depth of freezing

is the same as for melting. The simulated ice thickness is in contrast a combination of surface and bottom melting. From the strong surface melt in the model, I expect that the heat input of the air is overestimated in the model. I would suspect a slower complete desalination of the top layers in the simulation if the heat flux would be better represented because less fresh melt water would be available for vertical and horizontal flushing and therefore desalination of the upper layers.

On the other hand, I would not expect a better surface-ablation representation in the model to enlarge the agreement between the measurements and the simulation. The surface melting do not influence physical processes of the complex flushing approach, because the deviation from the measurements originates from the convection within the ice. The convection of the underlying water may caused higher liquid fractions, homogeneous temperatures and a high salinity in the interior and not only in the bottom layer. A simple parameterization approach introduced in Griewank and Notz (2015) which just includes vertical flushing was also tested to simulate the results of **Exp_20_1** (not shown) but it also could not better simulate the measurements.

12 Conclusion

Sea ice is continuous in temperature, salinity and solid fraction. Gravity drainage and flushing lead to a desalination during freezing and melting. The proceeded experiments provide a unique set of continuous measurements of these processes which are poorly understood so far. The so-called wireharp was found to be an appropriate measuring device for observing the bulk salinity evolution in thin sea ice in situ, specially in a laboratory environment.
Across the different experiments, the measured profiles almost show an half-shaped C-profile for solid fraction and bulk salinity, whereby a uniform low salinity can be found in the interior of the ice and a strong increase towards the bottom is present in the the lowest 4 cm of the ice. The newly forming ice at the bottom was assumed to have the salinity of the underlying water. In contrast to the lab measurements, Arctic ice cores of first-year ice show a C-shape (e.g Nakawo and Sinha, 1981), so a higher salinity at the ice surface. One explanation attempt in literature is a delay in the onset of gravity drainage which was found in laboratory and CTD measurements by Wettlaufer et al. (1997 and 2000). I did not find a temporal delay between reaching the freezing temperature of the water at the surface and the increase of water salinity in the CTD measurements. On the other hand, the wireharp has a vertical resolution of 2 cm and needed to be installed 2 cm under the water surface. Therefore the solid fraction and salinity for the upper most 2 cm remain unknown and the question if such an delay in desalination happened, cannot be answered completely.

As laboratory measurements offer only a limited setup of boundary conditions, I used the laboratory measurements to investigate how well a model can simulate the desalination during freezing. I used SAMSIM, a 1-D sea-ice model including the respective physical processes to simulate desalination during freezing. I forced the model with ice-surface temperatures and boundary conditions, measured in the cooling chamber. The simulated and measured ice thickness and temperature profiles do not differ more than 2 hours for thickness and about 0.1 °C for temperature. SAMSIM simulates a C-shape for S_{bulk} and reversed for Φ whereas the lab measurements only show a half C-shape. Either the measurements only start in 2 cm ice depth, it cannot be said if a full C-shape has developed in the artificial sea ice. The measured values of the interior sea-ice salinity are generally about 2-5 g/kg lower than the simulated salinity. This coincides with a slight underestimation of the simulated solid fraction. Due to the good agreement in shape of the profiles, I would argue that this is rather a physical misunderstanding of gravity drainage in SAMSIM than

caused by the choice of free parameters in the parameterization which were found by lab measurements of Notz et al. (2005). An improvement could be obtained by tuning the free parameters with a number of experiments conducted under very similar boundary conditions.

In contrast to ice-core measurements which only can cover a small fraction of time and space I used three wireharps to observe the temporal salinity evolution at different spots in the tank to investigate the homogeneity of the artificial sea ice. The measurements of the three wireharps were simulated with the respecting ice-surface temperatures. A comparison between measurements and simulations show a high agreement in ice thickness and ice temperature. The ice-surface temperature was not homogeneous across the tank, the total gradient in simulated surface temperature between the coldest and the warmest location was about 3 °C. From the bulk-salinity profiles, it can be seen that the ice at the coldest location entrapped more salt during freezing than at the warmer locations, what corresponds to findings of Notz et al. (2005). The comparison between the three locations showed, that SAMSIM is not very sensitive to the differences in ice temperature and simulates almost the same salinity profile for all three locations, whereas it overestimates the salinity at the two warmer locations by about 5 g/kg. In total values of bulk salinity, simulation and measurements agree the best for the coldest location. I would expect, that a collection of experiments for different freezing temperatures could help to enhance SAMSIM's sensivity to slightly changing boundary conditions.

To generate stable conditions in the artificial sea ice, the air temperature was set to a value which was supposed to create a stable ice thickness. This period of stabilization took about 2 days. As a result, the temperature gradient within the ice decreased, and the salinity as well as the solid fraction profile 'buckled' to a lower bulk salinity in the interior of the ice, whereas the ice in the upper most measured layer increased slightly. A reason for that could be brine redistribution within the ice but nothing can be said significantly as the salinity and solid fraction of the upper most 2 cm remain unknown. Further, these findings could explain the reason of C-shapes found in Arctic ice cores for sea ice, thicker than 30 cm. The higher salinity at the ice surface would then not be caused by a delay in the onset of gravity drainage rather by a redistribution of brine in the interior as the ice becomes thicker.

The collected measurements of the wireharp during melting are the first continuous measurements. The results therefore offer an observation of physical processes

which are almost unknown so far. The melting in the cooling chamber was introduced by setting the air temperature to +5 °C as the ice had grown to about 18 cm. The ice melted completely within 72 hours and the temperature gradient within the ice already disappeared in about 15 hours. Additionally the ice melted mostly from the bottom, surface melting did not exceed 2 cm as the wireharp was still covered by water in the end of the experiment. It was found, that there is a period during melting where the solid fraction sligthly increases in the upper layers. During this period, the temperatures in the upper most 2 cm increased to about -1.5 ± 0.1 °C an the salinity decreases. So the upper layers did experience a slight desalination. Afterwards, the ice melted at all layers as the resistance did not only decrease chronologically in the respective depths for decreasing ice thicknesses. Moreover as the ice became thinner than 12 cm, melting occured in all layers and the bulk salinity increased to 20 - 25 g/kg in the interior of the ice. I would assume the reason to be convection which replaced melt water with salty water from below. However it was not trivial to determine the ice thickness during melting, I assume the reason to be that the ice became very rugged in the end of melting

The melting process was simulated with SAMSIM, by implementing a positive atmospheric heat flux. The complex flushing approach of flushing introduced by Griewank and Notz (2015) assumes vertical and horizontal flushing, as it was found in ice-core measurements by Eicken et al. (2002). Brine is vertically flushed by melt water from the top and horizontally moving brine reaches cracks in the ice and flows directly in the underlying ocean. SAMSIM transports horizontal brine fluxes directly in the lowest layer. Furhermore, SAMSIM does not simulate the measured homogeneous temperature profile, either it generates a surface temperature of 0 °C. This goes along with a deeper and deeper completely desalination of the upper layers whereas I only measured a slight desalination in the upper layers. SAMSIM also only simulates an increase of bulk salinity in the lowest 4 cm of ice due to flushed salty brine from upper layers. It does not simulate the relatively high salinites in the interior, measured in the laboratory, as it does not assume a replacement of melt water by sea water. From these findings, I would concluded that SAMSIM's flushing parameterization is currently not able to simulate melting of very thin sea ice as it grew in the cooling chamber.

The measured profiles of solid fraction and bulk salinity during melting could be the basis of an improvement of the current flushing parameterization of SAMSIM. I would expect that the current state of the GSMs is far away from including a flushing

parameterization as it's improvements would be infinitesimal small in comparison to the computational time and cost. Contrary, 1-D models like SAMSIM offer a fast and easy way to enhance the understanding of physical processes. A higher accuracy of the solid fraction and also other properties of melting sea ice could help to improve satellite measurements. The uncertainty of sea-ice parameters, satellites can measure, is much higher in summer because the understanding of physical processes at the top and the interior of sea ice is worse than for winter. My measurements of the physical processes during melting occur on very small scales but they could contribute to improve large-scale observations.

Appendix

List of experiments

Experiment Name	Number of wire-harps	Cooling [°C]	Salinity [g/kg]	Heating wires W/m^2	Ice Core
Exp_15_1	1	-15	32	100	Yes
Exp_20_1	1	-20	33	100	Yes
Exp_15_3_A	3	-15	31.4	200	No
Exp_15_3_B	3	-15	31.2	200	No

Table 5. List of processed experiments. The name of experiment is composed as: **Exp _ Cooling temperature (positive) _ number of wireharps _ A/B**, (A/B: Experiment was repeated with similar boundary conditions).

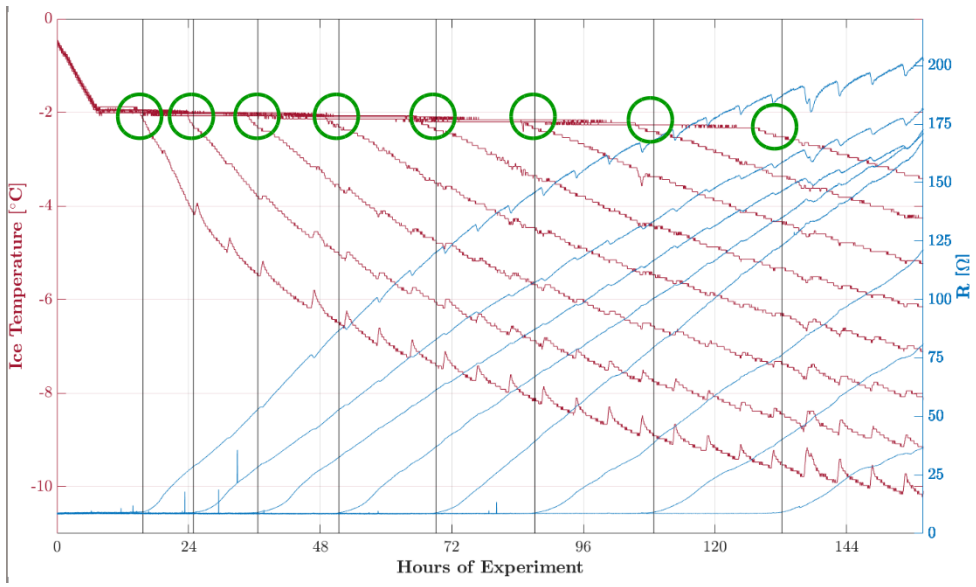

Figure 33. Temperature and resistance evolution of the freezing process. Start of ice growth derived by criteria from subsection 4.1 (black vertical lines) and ice growth derived by decreasing ice temperatures (green ellipses) coincidence.

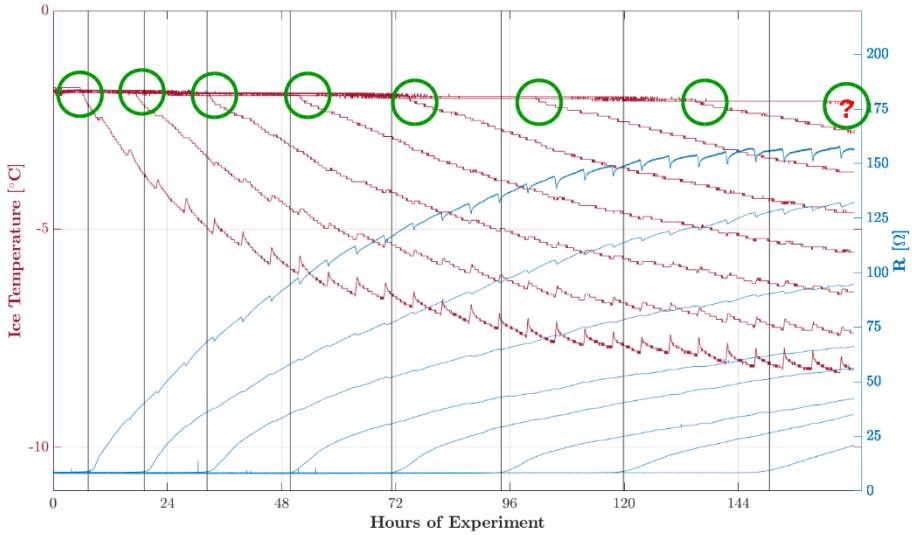

Figure 34. Temperature and resistance evolution for the freezing process. Start of ice growth derived by criteria from subsection 4.1 (black vertical lines) and ice growth derived by decreasing ice temperatures (green ellipses) do not coincidence. This leads to an error in temperature and depth of wirepair. The questionmark on the right-most side means, that the temperature drop cannot be seen for the shown time.

Data of the whole experiment, explained in section 6, section 9 and section 10

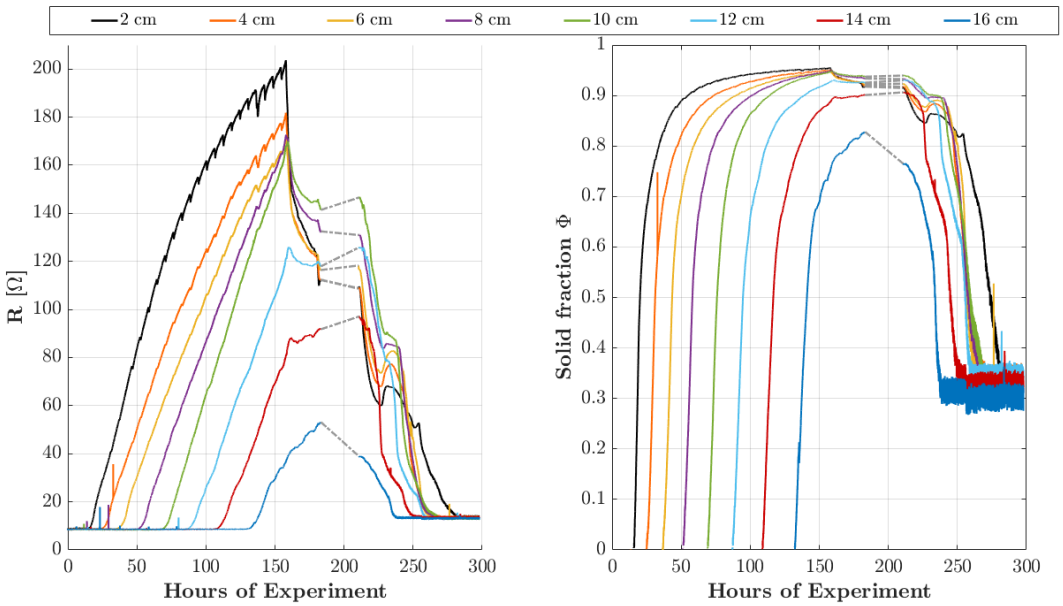

Figure 35. Resistance measurements R and Solid fraction Φ for freezing and melting. Cooling temperature, varying between-20 °C and -15 °C.

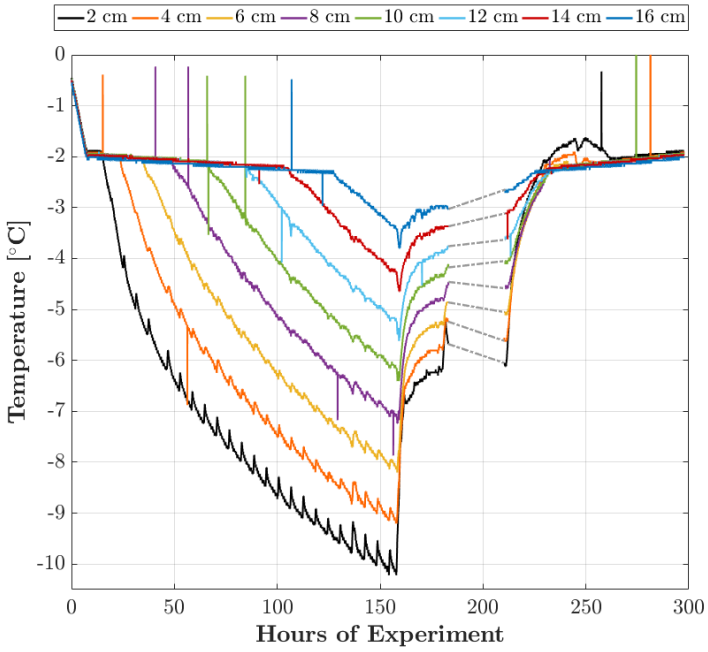

Figure 36. Temperature evolution for freezing and melting. Cooling temperature, varying between-20 °C an -15 °C.

Error estimation during melting for an offset in R

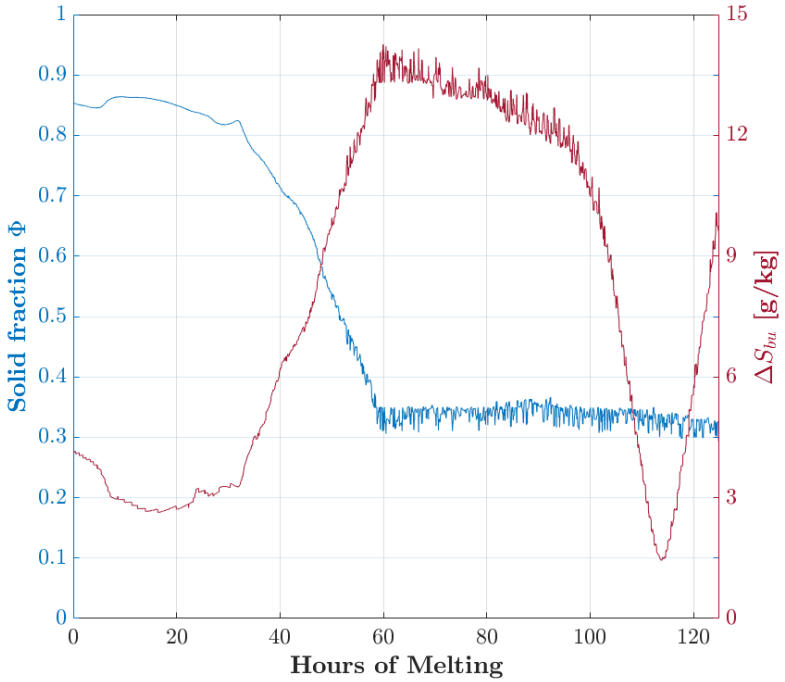

Figure 37. Solid fraction in 2 cm ice depth and ΔS_{bulk} for ΔR_0=5 Ω, for the melting process of **Exp_20_1**.

References

Aagaard, K. and E. C. Carmack (1989): "The role of sea ice and other fresh water in the Arctic circulation." In: *Journal of Geophysical Research* 94, pp. 14485–14498.

Assur, A. (1958): "Composition of sea ice and its tensile strength". In: *A. Nat. Acad. Sci./Nat. Res. Council, Arctic Sea Ice* 3213, 106–138.

Campbell, J. E. (1990): "Dielectric properties and influence of conductivity in soils at one of fifty megahertz." In: *Soil. Sci. Soc. Am. J.* 54(2), pp. 332–341.

Cottier, F., H. Eicken, and P. Wadhams (1999): "Linkages between salinity and brine channel distribution in young sea ice". In: *Journal of Geophysical Research: Oceans* 104.C7, pp. 15859–15871.

Cox, G. F. N. and W. Weeks (1975): "Brine drainage and initial sea entrapment in sodium chloride ice". In: *CRREL Re. Rep.* 345.

Eicken, H., M. A. Lange, G. S. Dieckmann (1991): "Spatial variability of sea-ice properties in the northwestern Weddell Sea". In: *J. Geophys. Res.* 96, pp. 10603–10615.

Eicken, H., T. C. Grenfell, D. K. Perovich, J. A. Richter-Menge and K. Frey (2002): "Hydraulic controls of summer Arctic pack ice albedo". In: *Journal of Geophysical Research: Oceans* 109.C8.

Feltham, D. L., N. Untersteiner, J. S. Wettlaufer and M. G. Worster (2006): "Sea ice is a mushy layer". In: *Geophysical Research Letters* 33(14).

Grenfell, T. C. and G. A. Maykut (2002): "The optical properties of ice and snow in the Arctic basin". In: *J.Glaciol.* 18(80), pp. 445–463.

Griewank, P. (2013): *A 1-D model study of brine dynamics in sea ice.*

Griewank, P. J. and D. Notz (2013): "Insights into brine dynamics and sea ice desalination from a 1-D model study of gravity drainage". In: *Journal of Geophysical Research: Oceans* 118.7.

Horner, R. (1985): "Sea Ice Biota". In: *CRC Press* Boca Raton, pp. 173–190.

— (1990): "Ice-associated ecosystems". In: *Medlin LK, Priddle J (eds).* In: Polar marine diatoms. British Antarctic Survey, Cambridge, p 9-14.

Jungclaus, J. H., N. Fischer, H. Haak, K. Lohmann, J. Marotzke, D. Matei, U. Mikolajewicz, D. Notz and J. S. Storch (2013): "Characteristics of the ocean simulations in the Max Planck Institute Ocean Model (MPIOM) the ocean component of the MPI-Earth system model". In: *Journal of Advances in Modeling Earth Systems* 5.2, pp. 422–446.

Kovacs, A. (1996): *Sea ice. Part 1, Bulk salinity versus ice floe thickness.* U.S. Army Cold Regions Research and Engineering Laboratory Hanover, N.H.

Krembs, C. and A. Engel (2001): "Abundance and variability of microorganisms and transparent exopolymer particles across the ice–water interface of melting first-year sea ice in the Laptev Sea (Arctic)". In: *Marine Biology* 138.1, pp. 173–185.

Nakawo, M and N. K. Sinha (1981): "Growth rate and salinity profile of first-year sea ice in the high arctic". In: *Journal of Glaciology* 27, pp. 315–330.

National Snow and Ice Data Center(NSIDC) (2018a): *Autumn freeze-up amps up*. URL: `https://nsidc.org/arcticseaicenews/`.

— (2018b): *Sea-ice characteristics: Salinity and Brine*. URL: `http://nsidc.org/cryosphere/seaice/characteristics/brine_salinity.html`.

Notz, D. and M. G. Worster (2008): "In situ measurements of the evolution of young sea ice". In: *Journal of Geophysical Research: Oceans* 113 (C3).

— (2009): "Desalination processes of sea ice revisited". In: *Journal of Geophysical Research: Oceans* 114.

Notz, D., J. S. Wettlaufer and M. G. Worster (2005): "A non-destructive method for measuring the salinity and solid fraction of growing sea ice in situ". In: *Journal of Glaciology* 51, pp. 159–166.

Perovich, D. K. (1998): "Observations of the polarization of light reflected from sea ice". In: *Journal of Geophysical Research* 103, pp. 5563–5575.

Stoessel, A., K. Yang and S.-J. Kim (2002): "On the role of sea-ice and convection in a global ocean model". In: *J. Phy. Oceanogr.* 32, pp. 1194–1208.

Tucker, W. B., A. J. Gow and W. F. Weeks (1987): "Physical properties of summer sea ice in the Fram Strait". In: *Journal of Geophysical Research: Oceans* 92.C7, pp. 6787–6803.

Untersteiner, N. (1968): "Natural desalination and equilibrium salinity profile of perennial sea ice". In: *Journal of Geophysical Research* 73(4), pp. 1251–1257.

Vancoppenolle, M., C. M. Bitz and T. Fichefet (2007): "Summer landfast sea ice desalination at Point Barrow, Alaska: Modeling and observations". In: *Journal of Geophysical Research: Oceans* 112 (C4).

Vaughan, D. G., J. C. Comiso, I. Allison, J. Carrasco, G. Kaser, R. Kwok, P. Mote, T. Murray, F. Paul, J. Ren, E. Rignot, O. Solomina, K. Steffen and T. Zhang (2013): "Climate Change 2013: The Physical Science Basis. Contribution of Working Group I to the Fifth Assessment Report of the Intergovernmental Panel on Climate Change". In: Stocker, T.F., D. Qin, G.-K. Plattner, M. Tignor, S.K. Allen, J. Boschung, A. Nauels, Y. Xia, V. Bex and P.M. Midgley (eds.). Cambridge University Press, Cambridge, United Kingdom and New York, NY, USA.

Wettlaufer, J. S., M. G. Worster and H. E. Huppert (1997): "Summer landfast sea ice desalination at Point Barrow, Alaska: Modeling and observations". In: *Journal of Geophysical Research: Oceans* 344 (C4), pp. 291–316.

Wettlaufer, W. F., M. G. Worster and H. E. Huppert (2000): "Solidification of leads: theory, experiment and field observations". In: *J. Geophys.Res.* 105(C(1), pp. 1123–1134.

Yang, Q, M. Losch, N. Svetlana, T. Jung, L. Nerger and T. Lavergne (2016): "Brief communication: The challenge and benefit of using sea ice concentration satellite data products with uncertainty estimates in summer sea ice data assimilation". In: *The Cryosphere* 10.2, pp. 761–774.

Acknowledgements

Ganz am Schluss möchte ich noch den Menschen danken, die diese Arbeit erst möglich gemacht haben. Als Allererstes natürlich Dirk Notz, für seine wissenschaftliche Unterstützung, Ermutigung, Positivität und Gelassenheit in den Momenten, in denen ich zu wenig davon hatte. Ich könnte mir wirklich keinen besseren Betreuer vorstellen. Danke auch an Johanna Baehr, für ihre Hilfe und die Freiheit, die Sie mir gelassen hat.

Ich bin sehr froh, die Erfahrung gemacht zu haben, selbstständig im Labor experimentieren zu dürfen. Das wäre allerdings nicht möglich gewesen ohne Leif Riemenschneider und Niels Fuchs, danke dass ihr immer wieder bereit wart, mir Dinge noch einmal zu erklären und mit mir nach Lösungen für Probleme zu suchen. Danke auch an Markus Ritschel, für seine Hilfe im Labor bei technischen Problemen oder einfach nur beim Putzen. Bedanken möchte ich mich auch bei Philipp Griewank, der mir immer zu Seite stand, wenn es Probleme mit SAMSIM gab und für seine Hilfe bei der Interpretation der Modelldaten. Unsere Telefonate haben mir immer viel Spaß gemacht.

Dank gilt auch sehr reichlich meiner Arbeitsgruppe, die mich den ganzen Weg der Arbeit begleitet, Feedback gegeben und alle Erfolge und Misserfolge geteilt hat. Danke vor allem an Clara Burgard, dass du dir die Zeit und Arbeit gemacht hast, meine Arbeit Korrektur zu lesen!

Ich möchte in diesem Zusammenhang auch meinen großartigen Kommilitonen danken, die mit mir alle Tiefen und Höhen der letzten 6 Jahre durchlebt haben und vor allem in der Zeit der Masterarbeit eine große Stütze waren. Ich würde mir wirklich niemand anderen wünschen, wenn ich die Zeit noch einmal durchleben könnte.

Vielen lieben Dank auch an Andrea Rochner und Karina Wiening, meinen großartigen Mitbewohnerinnen und Freundinnen. Ihr habt mich immer aufgefangen bei Misserfolgen und weiter an mich geglaubt. Danke auch an Markus Kraft, für die Freundschaft und das gemeinsame Leiden in den stressigen Phasen der Masterarbeit.

„Versicherung an Eides statt

Hiermit versichere ich an Eides statt, dass ich die vorliegende Arbeit im Studiengang M.Sc. Physikalische Ozeanographie selbstständig verfasst und keine anderen als die angegebenen Hilfsmittel – insbesondere keine im Quellenverzeichnis nicht benannten Internet-Quellen – benutzt habe. Alle Stellen, die wörtlich oder sinngemäß aus Veröffentlichungen entnommen wurden, sind als solche kenntlich gemacht. Ich versichere weiterhin, dass ich die Arbeit vorher nicht in einem anderen Prüfungsverfahren eingereicht habe und die eingereichte schriftliche Fassung der auf dem elektronischen Speichermedium entspricht. Ich bin mit der Ausstellung in der Fachbibliothek einverstanden.“

Hamburg, Luise Marie Zeigermann